# Gravity Model Explained by the Radiation Model in Modeling Epidemics

Hasitha Kuruvitage

Department of Mathematics

University of Colombo

*Supervisor*

Dr. H. C. Y. Jayathunga

Dr. Sandun Dassanayaka

In partial fulfillment of the requirements for the degree of

*Bachelor of Science in Applied Mathematics*

March 30, 2025

# Acknowledgements

I would like to express my heartfelt gratitude to my research supervisor, **Dr. H. C. Y. Jayathunga** of the Department of Mathematics, University of Colombo, and **Dr. Sandun Dassanayaka** of the Department of Decision Sciences, University of Moratuwa, for their invaluable guidance, encouragement, and support throughout this research.

I extend my special thanks to all the academic and non-academic staff in the Department of Mathematics for their assistance and for providing me with the necessary facilities to carry out this work.

Dedicated to my loving mother and father, who gives endless love and support.

# Abstract

Understanding the mechanisms behind human mobility patterns is crucial for improving the ability to predict the spread of infectious diseases. In this study, the modified gravity model and the radiation model are the most commonly used models for studying human mobility. The modified gravity model, based on Newton's law of universal gravitation, was used to predict human mobility between two locations by considering their population sizes and the distance between them. However, this model has certain limitations, such as requiring previous mobility data to fit the its parameters, and it is unable to predict human mobility between locations where systematic mobility data is unavailable.

In this study, the focus is the modified gravity model explained by the radiation model to derive the distance exponent parameter in the modified gravity model as a function of the properties of a population landscape to overcome the lack of systematic mobility data. Moreover, the radiation model is used to predict human mobility between locations to overcome the complexity of studying human mobility and the lack of systematic mobility data. It is also connected with the multi-patch SIRD model, in which the population is divided into compartments of susceptible, infected, recovered, and deceased, to study how human mobility affects the spread of infectious diseases in real-world

scenarios, such as the spread of COVID-19. This method can be used to study how human mobility influences the spread of any human-to-human infectious disease in the absence of systematic mobility data, and without considering mobility restrictions such as lockdowns. It also serves as a useful tool for informed decision-making in current and future public health.

# Contents

# List of Figures

# List of Tables

# Chapter 1

# Introduction

## 1.1 Motivations

Epidemiology is the study of the determinants and distribution of disease in a defined population. Epidemiology can accurately describe a disease and many factors concerning its spread before its cause is identified [1]. For example, during the early stages of the COVID-19 pandemic, before the specific cause of the virus was identified, epidemiologists used human mobility data to describe and predict its spread. Analysis of this data revealed how the virus spread from Wuhan, China. It also revealed that high levels of human mobility helped the virus spread and that limiting human mobility could control the spread of the virus [2]. This shows the importance of understanding human mobility patterns in studying the spread of infectious diseases.

But natural human mobility patterns are complex to understand, as they can occur on various time scales, depending on the context and factors driving the movement. For example, short-term movements are influenced by the daily work schedule, whereas long-term trends can be due to seasonal employment opportu-

nities. Moreover, there are multiple other reasons that also can change human mobility patterns, such as fear of diseases, political instability, etc.[3].

The interesting thing is the availability of mathematical models with some boundaries to understand human mobility patterns and study the spread of infectious diseases, considering human mobility patterns such as the radiation model, gravity model, modified gravity model, etc. [4; 5] and the multi-patch SIR model, multi-patch SEIR model, etc. [6; 7], respectively. Not only that, but the understanding gained from human mobility models can be used to connect these models and study how human mobility patterns affect the spread of infectious diseases.

The integration of these mathematical models with epidemiology not only helps to understand the spread of infectious disease, but it also helps in current and future decision-making in public health.

## 1.2 Context of the Study

Some mathematical models have been designed to cover the complexity of studying human mobility, among which the modified gravity model and the radiation model are the most commonly used. The modified gravity model, based on Newton's law of universal gravitation, was used to predict human mobility between two locations by considering their population sizes and the distance between them. However, this model has certain limitations, such as requiring previous mobility data to fit the its parameters, and it is unable to predict human mobility between locations where systematic mobility data is unavailable.

On the other hand, the radiation model overcome some of the limitations from the modified gravity model, whereby individuals are assumed to go for the closest job that meets a given level of expectations therefore, it gives more accurate predictions of human mobility for larger distances.

In this study, the focus is the modified gravity model explained by the radiation model to derive the distance exponent parameter in the modified gravity model as a function of the properties of a population landscape to overcome the lack of systematic mobility data. Moreover, the radiation model is used to predict human mobility between locations to overcome the complexity of studying human mobility and the lack of systematic mobility data. It is also connected with the multi-patch SIRD model, in which the population is divided into compartments of susceptible, infected, recovered, and deceased, to study how human mobility affects the spread of infectious diseases in real-world scenarios, such as the spread of COVID-19.

## 1.3 Overview of the Thesis

This thesis has been structured in five main chapters, as well as with additional tables, data sources and programming codes providing appendix. Chapter 1 introduces the motivation to use mathematical models in epidemiology studies, provides the reason behind why this study is being done and gives an overview of the thesis.

Chapter 2 provides the literature review of the key models used in this study, such as the modified gravity model, radiation model, Soneira-Peebles model, multi-patch SIRD model, Rescaled travel probability,etc., and previous studies

and findings which are important for this study. Moreover, the final part of this chapter clearly explains the objectives of the research.

The next chapter explains the mathematical and computational techniques used in this study. This chapter is divided into three main sections. The first section is "Connecting the Radiation-on-Landscape Model to the Modified Gravity Model". In this section consider a heterogeneous population landscape, which is the population of each patch following the power-law probability distribution, assuming the location and population of each patch are fully uncorrelated with each other. Moreover, the radiation model on such population landscapes, namely, the radiation-on-landscape (RoL) model, is written in terms of the distance between two patches. By expanding the rescaled travel probability in the RoL model and comparing it to the modified gravity model, derive the distance exponent in the modified gravity model as a function of properties of the population landscape. It also shows this distance exponent function can vary according to the population sizes of origin and destination patches. Here, a patch means a crowded area such as a community, city, country, etc.

The second section is "Understanding Human Mobility Patterns Between Provinces". In this section the variables of the radiation model will be estimated and used to estimate human mobility between provinces in Sri Lanka. The last section in chapter 3 is "Connecting Human Mobility Data With Multi-Patch SIRD Model". In this section, develop the connection between radiation model and multi-patch SIRD model

Chapter 4 presents the overview of COVID-19 in Sri Lanka, parameter values and initial conditions of the multi-patch SIRD model based on the COVID-19

context. Moreover, the last section of this chapter contains the results of the multi-patch SIRD model, which is connected to the radiation model in the last section of Chapter 3, and these results show the spread of COVID-19 between provinces in Sri Lanka. Moreover, the last chapter discusses the importance of results.

# Chapter 2

# State of the Art

## Summary

This chapter provides the literature review of the key models used in this study, such as the modified gravity model, radiation model, Soneira-Peebles model, multi-patch SIRD model, Rescaled travel probability,etc., and previous studies and findings which are important for this study. Moreover, the final part of this chapter clearly explains the objectives of the research.

## 2.1 Literature Review

### 2.1.1 Modified gravity model

One of the major laws of the natural sciences is Newton's law of universal gravitation. Newton's law of universal gravitation states that the force between two objects in the universe $F_{ij}$ is proportional to the product of the masses of the two objects $m_i$ and $m_j$ divided by the square of the distance $r_{ij}$ between the two objects below as [8]:

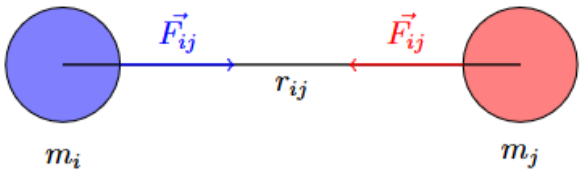


Figure 2.1: Newton's law of universal gravitation.

$$F_{ij} \propto \frac{m_i m_j}{r_{ij}^2}$$

Under epidemiology, Newton's law of universal gravitation model has similar usage which discussed above, but the usage objective is understanding human mobility patterns. According to the objective, $m_i$ is the population of patch $i$ (origin), $m_j$ is the population of patch $j$ (destination), $F_{ij}$ is the human flow from patch $i$, patch $j$ and $r_{ij}$ is the distance between patch $i$ and patch $j$.

The important point is that the distance exponent is not always exactly 2, it depends on various factors. For example, culture and language can significantly affect to the human flow from one patch to another patch. Consider a country with many languages and cultures then the distance exponent is significantly large. As distance increases, people encounter different cultures and languages, which reduces their tendency to travel. Now consider a country with a small number of languages and cultures then the distance exponent is smaller than before. This is because, even as distance increases, there are no significant differences in language and culture, and therefore the tendency of people to travel is not greatly reduced. The purpose of introducing distance exponent $\gamma$ is to allow for capture how other variables impact to the distance $r_{ij}$, then $F_{ij}$ proportional below as:

$$F_{ij} \propto \frac{m_i m_j}{r_{ij}^{\gamma}} \tag{2.1}$$

Now, consider two cities that have different economies. The potential to generate movement of higher-economic city is lower. As a city with a higher economic has more opportunities therefore, humans do not tend to go outer. But the potential to generate movement of lower-economic city is higher. As a city with a lower economic has limited opportunities therefore, humans tend to go outer. The purpose of introducing origin exponent $\theta$ is to allow for capture how other variables impact to the generation of human flow, except population of origin $m_i$.

Similarly, consider two cities that have different economies. The potential to attract movement of higher-economic city is higher. A a city with a higher economic has more opportunities therefore, humans tend to come. But the potential to attract movement of lower-economic city is lower. As a city with a lower economic has limited opportunities therefore, humans do not tend to come. The purpose of adding destination exponent $\omega$ to the is to allow for capture how other variables impact to the attraction of human flow, except population of destination $m_j$.

Therefore, two fundamental modifications need to be made to the basic model in Equation 2.1, then the modified gravity model [9; 10] shown below:

$$F_{ij} = k\frac{m_i^{\theta} m_j^{\omega}}{r_{ij}^{\gamma}} \tag{2.2}$$

Here $\theta$ is the potential to generate movement, $\omega$ is the potential to attract

movement and k is the proportionality constant. The effects of these exponents are graphed in Figure 1.2 in [9]. Moreover, the method to find the best values for the modified gravity model parameters has been discussed in [10].

Despite the widespread use of modified gravity models, it has notable limitations [10] for example:

1. The modified gravity model cannot account for fluctuations in the number of travelers between two locations.

2. Equation 2.2 predicts that the human flow increases without limit as increases the destination population $m_j$, but the human flow cannot exceed the origin population $m_i$.

3. Equation 2.2 requires previous mobility data to fit the parameters $\theta, \omega, \gamma$, it is unable to predict human mobility when the lack systematic mobility data.

4. The modified gravity model gives same predictions for two pairs of locations with similar origin and destination population sizes with similar distance.

### 2.1.2 Radiation model

Motivated by above limitations which discussed under modified gravity model for introducing a new model to over come limitations (1)-(4). This new model is called radiation model and it is based on the two assumption that employees seek the closest job which meets their expectations. The assumptions are below as [10]:

(1) An individual seeks job offers from all patches, including his/her home patch. The number of employment opportunities in each patch is proportional to the patch's population, assuming that there is one job opening for every $m_{job}$

individuals then each patch with population $m$ has $m/m_{jobs}$ employment opportunities. The benefits of an employment opportunity are represented by a single value $z$, randomly chosen from distribution $p(z)$ where $z$ represents a combination of income, working hours, conditions, etc. Thus, each of these $m/m_{jobs}$ employment opportunities is assigned $m/m_{jobs}$ random numbers, $z_1, z_2, ....., z_{m/m_{jobs}}$ to represent its specific benefits.

(2) The individual chooses the closest job to his/her home, whose benefits $z$ are higher than the best offer available in his/her home patch. Thus lack of commuting has priority over the benefits, i.e. people are willing to accept staying close to home more than getting a job with better benefits.

This process, applied in proportion to the population in each patch, assigns work locations to each individual, which in turn determines the daily humans' flow across the country. Moreover, the model has three unknown parameters such as the benefit distribution $p(z)$, the job density $m_{jobs}$ and the total number of commuters $M_c$. However, that the average humans' flow (average number of commuters) from one location to another location are independent of $p(z)$ and $m_{jobs}$ and the remaining free parameter $M_c$ does not affect the flow distribution therefore, the radiation model is parameter free [10].

Consider patch $i$ (origin) and $j$ (destination) with population $m_i$ and $m_j$ respectively, at distance $r_{ij}$ between each other then defined $s_{ij}$ is the total population in the circle of radius $r_{ij}$ centered at patch $i$ excluding the origin and destination population. According to the above assumptions, the average human flow (average number of commuters) $T_{ij}$ from $i$ to $j$, as predicted by the radiation model below as:

$$T_{ij} = T_i \frac{m_i m_j}{(m_i + s_{ij})(m_i + m_j + s_{ij})} \tag{2.3}$$

Which is independent of both $p(z)$ and $m_{jobs}$. Here $T_i \equiv \sum_{j \neq i} T_{ij}$ is the total number of commuters that start their journey from patch $i$ and it is proportional to the population of the origin. Moreover, $T_i = m_i(M_c/M)$ where $M$ is the total population in the country [10].

Note that a key difference between the radiation model and the modified gravity model is that the radiation model has not distance terms $r_{ij}$ but has $s_{ij}$. Thus the human flow depends not only on $m_i$ and $m_j$ but also on the population $s_{ij}$ of the region surrounding the origin. Moreover, the radiation model has several advantages compared to the modified gravity model such as clear theoretical background, universality due to the absence of parameters to be estimated, better prediction for long-distance travels, despite some unresolved issues like relatively poor predictability on short-distance travel,etc [11].

Although the radiation model doesn't seem to be the most appropriate one for predictions at small scale units, it can be implemented successfully at larger scales therefore, a patch represent by a large area such as metropolitan areas, provinces, cities, etc. [12].

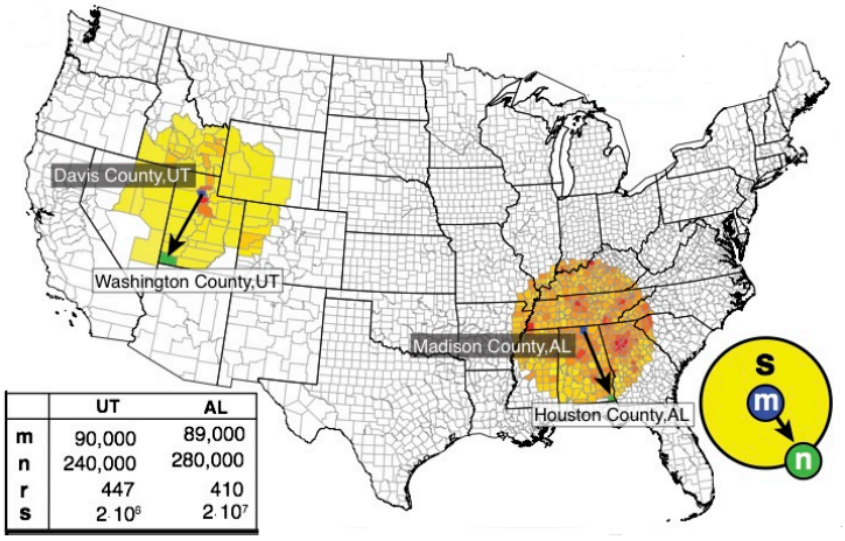


Figure 2.2: Graphical representation of an example for the radiation model.

The Figure 2.2 shows the two pair of origin and destination in United States with their populations $m_i$ and $m_j$ respectively, distance between each other $r_{ij}$ and corresponding surrounding population $s_{ij}$ [10].

### 2.1.3 Rescaled travel probability

The radiation model in Equation 2.3 which discussed under radiation model can use to define the travel probability from patch $i$, $j$ given by [11]:

$$P_{ij} = \frac{T_{ij}}{T_i} = \frac{m_i m_j}{(m_i + s_{ij})(m_i + m_j + s_{ij})} \tag{2.4}$$

Furthermore, rescaled travel probability from patch $i$,$j$ given by [11]:

$$\frac{P_{ij}}{m_i m_j} = \frac{1}{(m_i + s_{ij})(m_i + m_j + s_{ij})} \tag{2.5}$$

### 2.1.4 Power-law function

The power-law function $f : D \subseteq \mathbb{R} \to \mathbb{R}$ has nice relationship between dependent variable $f(x)$ and independent variable $x$ such as $f(x) \propto x^{\alpha}$,$\alpha$ is called power-law exponent and $D$ depends on the context. Therefore, the general form of power-law function is $f(x) = kx^{\alpha}$ here $k$ is proportionality constant. Consider the area of a square region in terms of the length of its side. If double the length then multiply the area by a factor of four. This example has a power-law relationship and it shows one of important property of power-law function i.e. $f(bx) = b^{\alpha} f(x)$ for $b \in \mathbb{R}, x \in D$.

According to the above example $f(x)$ is the area of square region when $x$ is the length of its side and $D = (0, \infty)$.The below graphs show how the shape of $f$ changes with different $\alpha$.

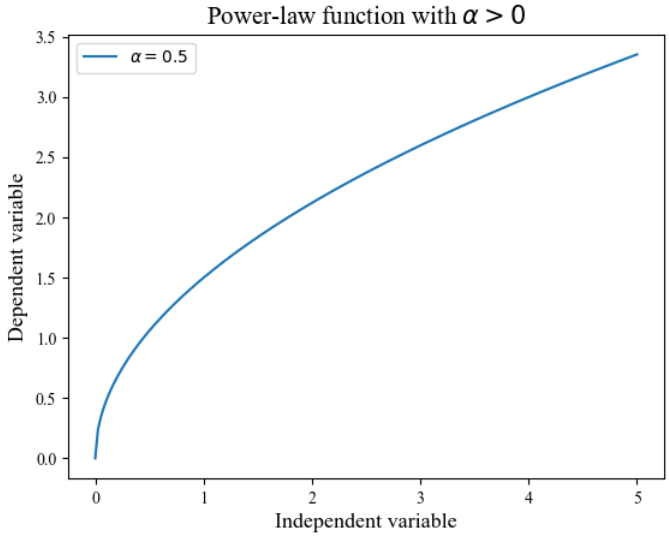


Figure 2.3: Shape of power-law function when power-law exponent bigger than zero.

This Figure 2.3 shows the shape of $f$ when $\alpha > 0$. The integral $\int_{x_{min}}^{\infty} f(x)\, dx$

is not bounded for any $x_{min} > 0$.

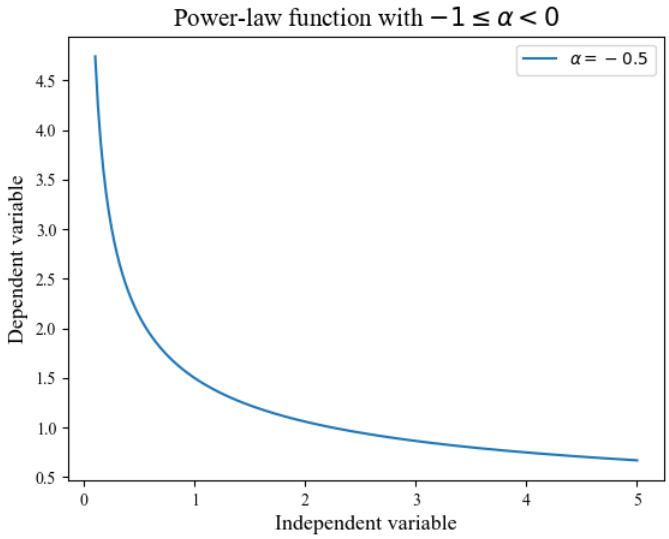


Figure 2.4: Shape of power-law function when power-law exponent bigger than or equal -1 and less than zero.

The Figure 2.4 shows the shape of $f$ when $-1 \leq \alpha < 0$. The integral $\int_{x_{min}}^{\infty} f(x)\,dx$ is not bounded for any $x_{min} > 0$.

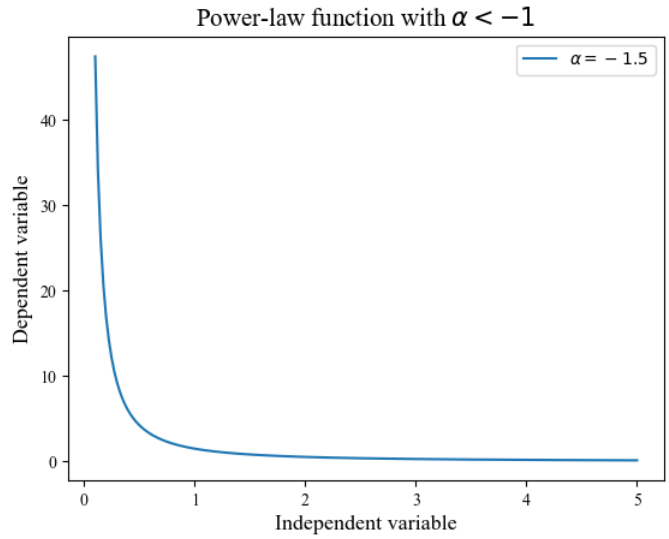


Figure 2.5: Shape of power-law function when power-law exponent less than -1.

The Figure 2.5 shows the shape of $f$ when $\alpha < -1$. The integral $\int_{x_{min}}^{\infty} f(x)\,dx$ is bounded for any $x_{min} > 0$.

The Figures 2.3,2.4 show $f$ cannot be defined as a probability distribution. However, the Figure 2.5 shows $f$ can be defined as a probability distribution on $[x_{min}, \infty)$ below as:

$$f(x) = (\beta - 1)x_{min}^{\beta-1}x^{-\beta} \tag{2.6}$$

when power-law exponent $\beta > 1$,$x_{min} > 0$ and the proportionality constant $k$ ensure that the $\int_{x_{min}}^{\infty} f(x)\,dx = 1$ as required by a probability distribution [13]. The way of finding power-law exponent $\beta$ for a probability distribution explain in [13; 14].

Moreover, the Equation 2.6 is called power-law probability distribution and more than a hundred power-law probability distributions have been identified in physics (e.g.Sandpile avalanches [15]), biology (e.g.species extinction and body mass [16]), social science (e.g. city sizes and income [17; 18]),etc.

### 2.1.5 Fractal dimension

Fractal dimension is (usually) a non- integer number which measures complexity, roughness or irregularity of an object with respect to the space in which the it lies [19]. There are several type of fractal dimensions for different contexts such as similarity dimension [20], Correlation dimension [21],Hausdorff dimension [22], etc.

Moreover, many objects have a property of self-similarity i.e. an object is self-similar if there is a point where every neighborhood of the point contains a

copy of entire object [20]. For example, imagine the figure formed by inscribing a square within another square, rotated by $45^0$. Then inside the inner square, inscribe another square in the same manner. The figure of the above example cannot be accurately drawn, since it contains infinitely many nested squares, but an approximation of the result is shown below:

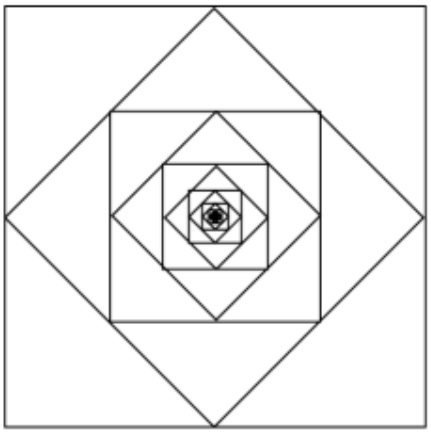

Figure 2.6: An example for the self-similar object.

The Figure 2.6 shows an object has self-similar at the center of the squares – every ball around the center, no matter how small, will contain a complete copy of the entire figure. However, this is the only point where the figure is self-similar [20].

An object is strictly self-similar if it is self-similar at every point. Equivalently, this means that the object can be decomposed into some number of disjoint pieces, each of which is an exact copy of the entire object [20].

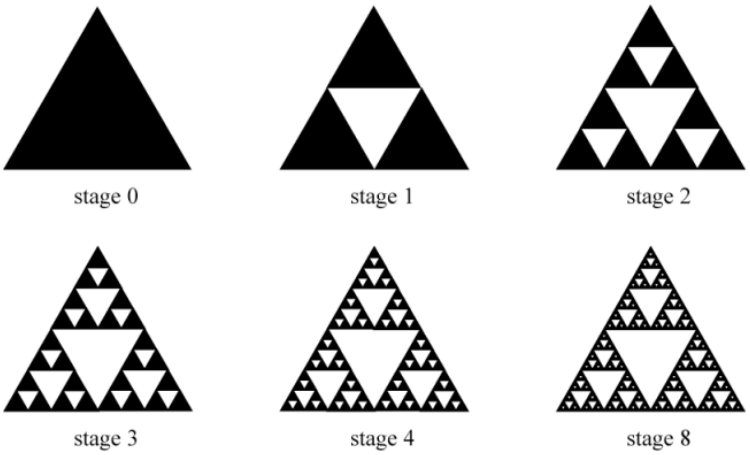


Figure 2.7: An example for the strictly self-similar object.

The Figure 2.7 shows an example for a strictly self-similar object (Sierpinski triangle). Starting with a filled equilateral triangle, it is divided into four smaller triangles by connecting the midpoints of its sides and the central triangle is removed. This process is repeated for each remaining smaller triangle. Therefore, this object can be decomposed into some number of disjoint pieces, each of which is an exact copy of the scaled-down version of entire object [20].

A definition that is useful for strictly self-similar objects, called the similarity dimension [20]. This definition is based on the fact that these objects can be cut into pieces identical to the original object, but scaled by some factor. The question is then how to relate the number of pieces the original was figure cut into and the scaling factor.

To understand this relationship, first consider our simplest geometric objects such as line segment, square and cube in dimensions 1,2 and 3 respectively. Scale each of these objects by a factor of 1/2. The number of the smaller copies do you need to assemble to get the original object show below as:

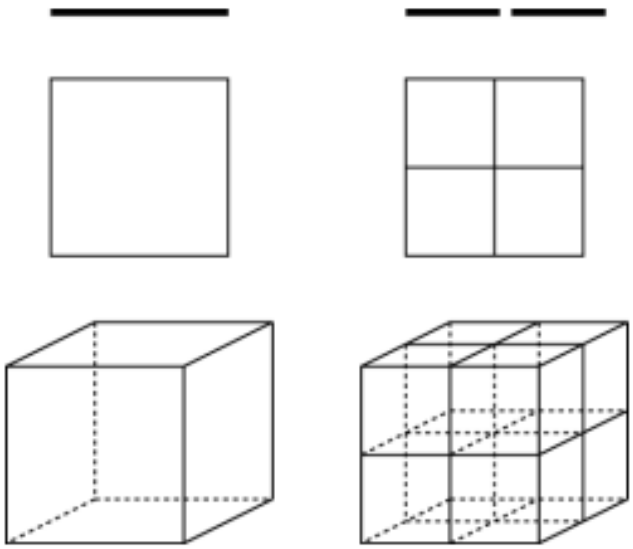

Figure 2.8: Graphical representation of finding the dimension of an strictly self-similar object.

The Figure 2.8 shows if you scale by a factor of $1/k$, the line segment requires $k$ copies, the square requires $k^2$ copies, and the cube requires $k^3$ copies. This indicates that if you take a $d_f$ dimensional figure and scale it by a factor of 1/k, you will need $k^{d_f}$ copies to recreate the original object [20].

So if have a strictly self-similar object which can decompose into $n$ pieces, each of which is a copy of the original object scaled by a factor of $1/k$, then [20]

$$n = k^{d_f}$$

$$log(n) = d_f log(k)$$

$$d_f = \frac{log(n)}{log(k)}$$

here $d_f$ is called similarity dimension. Moreover, fractal dimension has been studied in almost every field of science and engineering including mathematics,

computer science, physics, chemistry, biology, geology, social science, economics, engineering, technology, art, architecture, etc [23]. Fractals and their applications have high potential to expand further encompassing many interdisciplinary and evolving fields of research.

### 2.1.6 Modeling heterogeneous population landscapes

For modeling a heterogeneous population landscape, first generate a set of patches in two-dimensional space using Soneira-Peebles model. The Soneira-Peebles model originally developed for simulating the self-similar galaxy distribution [24].This model in two-dimensional space is controlled through three parameters $\lambda > 1$ is called contraction factor,$L$ is the number of layers and $\eta$ is the number of patches in first layer. Moreover, it is discussed below as [25]:

(1) The first layer is a circle of radius $R$ is generated as a starting point.

(2) The second layer is a set of $\eta$ circles with radius $R/\lambda$ such that center of each circle placed in randomly on previous layer.

(3) The third layer is also a set of $\eta^2$ circles with radius $R/\lambda^2$ such that exactly centers of $\eta$ circles placed in randomly on one of circle (radius = $R/\lambda$) in previous layer. Similarly other centers of $\eta^2 - \eta$ circles are distributed through the rest of circles in previous layer.

(4) This process is repeated until $L^{th}$ layer, then the $L^{th}$ layer has $\eta^L$ centers.

According to the context a center is defined as a patch. The figure below shows the graphical representation of an example of the first two layers of patches

generated using the Soneira-Peebles model in two-dimensional space.

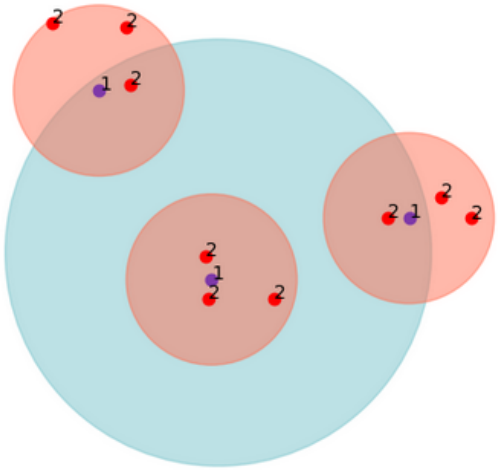

Figure 2.9: Graphical representation of an example of the first two layers of patches generated using the Soneira-Peebles model in two-dimensional space.

The Figure 2.9 shows the graphical representation of an example of the first two layers of patches generated using the Soneira-Peebles model in two-dimensional space when $\eta = 3, R = 1$ and $\lambda = 3^{1/1.2}$. The number in each patch denotes the layer which it belongs to. The patches at the first layer (blue) are randomly placed within the circle with radius $R = 1$. Similarly, the patches at the second layer (red) are randomly placed within the circles with radius $R/\lambda$.

According to the context, use similarity dimension $d_f$ to measure the complexity of set of patches which generated in two-dimensional space using Soneira-Peebles model. Moreover, $d_f$ depends on the parameters $\eta$ and $\lambda$ in following way [25]:

$$d_f = \frac{log(\eta)}{log(\lambda)} \tag{2.7}$$

From Equation 2.7, the contraction factor $\lambda = \eta^{1/d_f}$ therefore, the radius

$R/\lambda^k$ of circles in layer $k+1$ depends on $d_f$. It shows that $d_f$ can effect to the clustering of patches, the graphs below show how it effects.

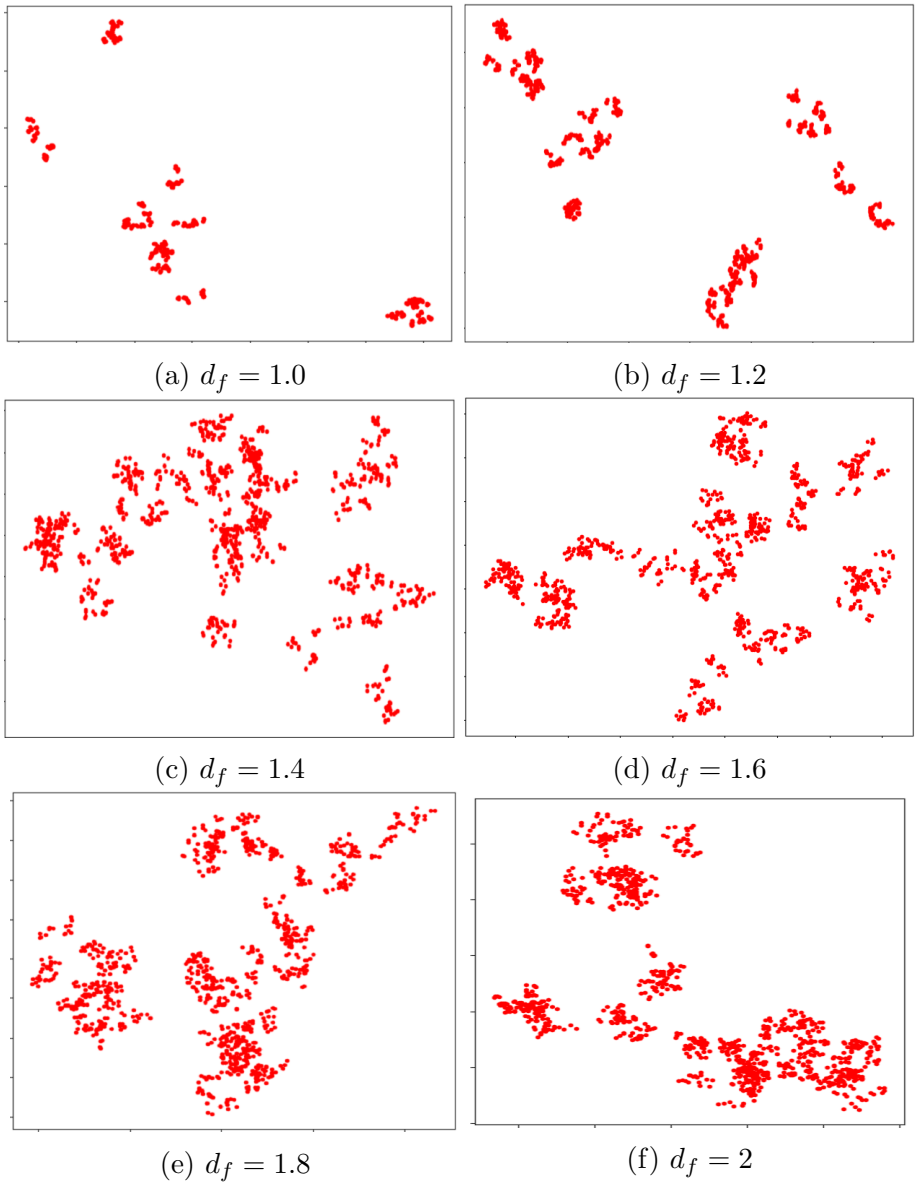

(a) $d_f = 1.0$ (b) $d_f = 1.2$

(c) $d_f = 1.4$ (d) $d_f = 1.6$

(e) $d_f = 1.8$ (f) $d_f = 2$

Figure 2.10: Sets of patches simulated from Soneira-Peebles model for different values of the similarity dimension $d_f$ in the range 1-2.

The Figure 2.10 shows an example for sets of patches simulated from Soneira-Peebles model for different values of the similarity dimension $d_f$ in the range 1-2.

Each set contains 1024 patches. One can see that decreased clustering level is related to bigger value of $d_f$.

The power-law probability distribution $f$ which disused under power-law function can use to assign random population $m \geq m_0$ for each generated patch, buy generating random number $f(m) \in (0, f(m_0))$ and substitute to the Equation 2.8

$$m = \left[ \frac{(\beta - 1) m_0^{\beta - 1}}{f(m)} \right]^{1/\beta} \tag{2.8}$$

.

here $m_0$ is the minimum of the population [11]. The Figure 2.11 shows an example of generated heterogeneous population landscape using Soneiral-Peebles model and power-law probability distribution.

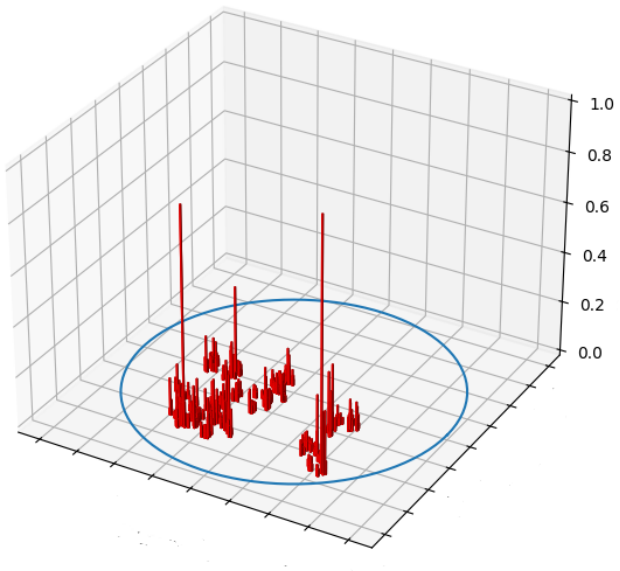


Figure 2.11: An example of generated heterogeneous population landscape using Soneiral-Peebles model and power-law probability distribution.

The Figure 2.11 shows an example of generated heterogeneous population

landscape using the Soneira-Peebles model and power-law probability distribution when $\eta = 2, \lambda = 2^{1/1.2}, L = 10, d_f = 1.2, R = 1$,power-law exponent $\beta = 3$ and the minimum of the population $m_0 = 100$. The hight in the vertical axis represents the normalized value of the population assigned to each patch.

### 2.1.7 Multi-patch SIRD model

Much of the mathematical study of the spread of infectious diseases start from the classic compartment models of [26; 27]. These models divide the population into several different compartments (e.g., susceptible,infective,recovered,..) and specify how agents move across the separate compartments over time. The SIRD epidemic model discussed in this paper is one of the simplest compartmental models [28]. [29] presents a useful overview of this class of models and some of their theoretical properties and [30] shows how to apply optimal control methods to them. Also, [31] is a recent, comprehensive textbook of the field and [32] is an example of how these models have been applied to understand the current health crisis by epidemiologists.

Under the SIRD epidemic model categorizes a population into four classes of individuals representing four distinct states of the pandemic such as Susceptible $S(t)$, Infected $I(t)$, Recovered $R(t)$ and Death $D(t)$ in period $t$. The susceptible group does not yet have immunity to disease and individuals in this group have the possibility of getting infected. On the other hand, the recovered group consists of individuals who are immune to the disease and finally, $D(t)$ represents individuals who have succumbed to the disease.

The Susceptible-Infected-Recovered-Death (SIRD) model builds on the principle that the fraction of the infected individuals in the population $I(t)/N$ can

transmit the disease to susceptible ones $S(t)$ with the infection rate of $\beta$, here $N$ is the total population. Therefore, the number of newly infected individuals in the current period $t$ is $\beta(I(t)/N)S(t)$. The newly infected individuals, that is confirmed cases in period $t$ should be deducted from the susceptible individuals in the current period $t$. Moreover, in each period $t$, the fraction $\alpha$ of the infected people recover from the disease, which reduces the number of actively infected individuals. Similarly, in each period $t$ the fraction $\mu$ of the infected people have succumbed to the disease, further reducing the number of actively infected individuals. Hence, in period $t$ the fraction $\alpha + \mu$ of the infections are resolved in total [33].

According to the above dynamics of infectious disease, the structure of SIRD model shows below as:

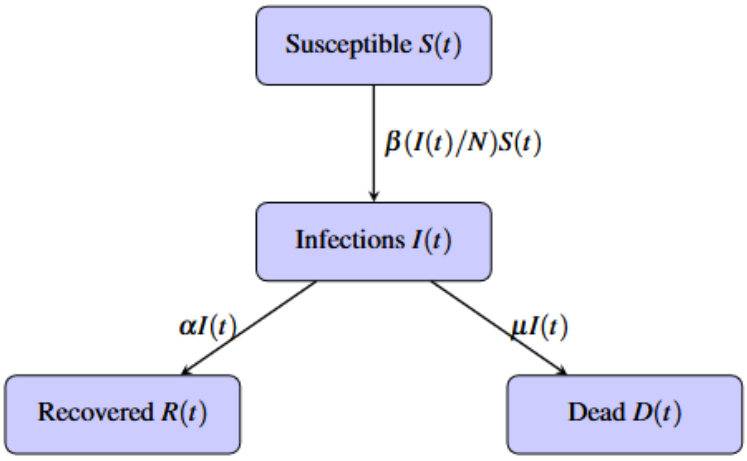


Figure 2.12: Structure of the SIRD model.

According to the structure of SIRD model, the SIRD model can be defined as a set of differential equations (ODE) below as [34]:

$$\frac{d}{dt}S(t) = -\frac{\beta S(t)I(t)}{N} \tag{2.9}$$

$$\frac{d}{dt}I(t) = \frac{\beta S(t)I(t)}{N} - \alpha I(t) - \mu I(t) \tag{2.10}$$

$$\frac{d}{dt}R(t) = \alpha I(t) \tag{2.11}$$

$$\frac{d}{dt}D(t) = \mu I(t) \tag{2.12}$$

with initial values $S(0) > 0, I(0) > 0, R(0) \geq 0$ and $D(0) \geq 0$. Moreover, the SIRD model is based on 6 basics assumptions [34] such as:

1. The recovered people will no longer be susceptible to infection again.
2. the number of deaths due to other causes is neglected,
3. The area under study is closed and isolated from other areas i.e. $N(t) = S(t) + I(t) + R(t) + D(t)$,
4. people are identical to each other (i.e. different demographic factors or health conditions are not considered).
5. The effect of the vaccination campaign does not depend.
6. Tndividual populations are randomly distributed over the area, allowing for a fixed identification of communication between those exposed to infection and the injured.

Generally the SIRD model [28; 33; 34; 35; 36] is used for describe the spread of infectious diseases in a single patch. However, the SIRD model can modified to a multi-patch compartment model is used to describe the spread of infectious disease when individuals are moving between different patches, assuming people can move between patches, bringing the pathogens along. Rather than knowing that people are just in one patch, mainly this model consider movement between patches and how that affects the spread of infectious disease.

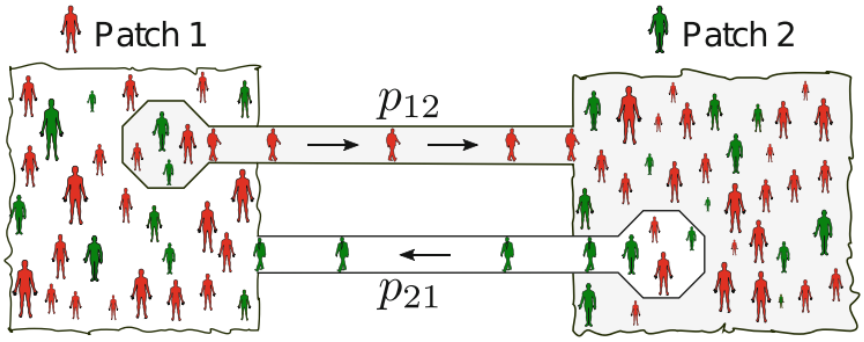


Figure 2.13: An example of showing how human mobility impacts the spread of infectious disease between two patches.

The Figure 2.13 shows how human mobility impact to the spread of infectious diseases between patches. Initially patch 1 contains both susceptible, infected individuals and patch 2 contains only susceptible individuals. After moving individuals from patch 1 to patch 2, disease is spread in patch 2.

Moreover, the risk of spread of infectious disease in a patch can be different each other base on its properties. For example, a highly populated patch would have a higher risk to spread of infectious disease speed than in lower populated patch. Therefore, the spread of infectious disease in a patch can be different each other. The multi-patch SIRD compartment model below as [7]:

$$\frac{d}{dt}S_i(t) = -S_i(t)\sigma_i \tag{2.13}$$

$$\frac{d}{dt}I_i(t) = S_i(t)\sigma_i - \alpha_i I_i(t) - \mu I_i(t) \tag{2.14}$$

$$\frac{d}{dt}R_i(t) = \alpha_i I_i(t) \tag{2.15}$$

$$\frac{d}{dt}D_i(t) = \mu I_i(t) \tag{2.16}$$

where $S_i(t)$, $I_i(t)$, $R_i(t)$ and $D_i(t)$ denote the population of susceptible, infected, recovered and disease-induced death individuals respectively, in patch $i$ in period $t$. The parameters $\alpha_i$ denotes the per-capita recovery rate in patch $i$ and $\mu_i$ denotes the disease-induced death rate in patch $i$. The infection rate $\sigma_i$ in patch $i$ have the form below as [7]:

$$\sigma_i = \sum_{j=1}^{n} \beta_j W_{ij} \frac{\sum_{k=1}^{n} W_{kj} I_k}{\sum_{k=1}^{n} W_{kj} N_k} \tag{2.17}$$

with $W_{ij}$ denotes the proportion of individuals from patch $i$ who are currently in patch $j$ , $\beta_j$ is the risk of infection in patch $j$ , and the last fraction represents the proportion of infected in patch $j$.

These multi-patch compartment models [6; 7; 37; 38; 39] allow scientists and health officials to get a better understanding of how infectious diseases spread

in a wide-scale area like a country with human mobility and what strategies can explore to manage an outbreak.

## 2.2 Previous Studies and Findings

In [11], they study the more fundamental connection between the radiation and gravity models in a realistic population landscape. In order to study such a connection, first they model the heterogeneous population landscape using Soneiral-Peebles model with assuming the population of each patch following the power-law probability distribution. Then the radiation model on such population landscapes, namely, the radiation-on-landscape (RoL) model, can be written in terms of the distance between two patches. By expanding the rescaled travel probability in the RoL model and comparing it to the gravity model, they derive the distance exponent in the gravity model as a function of the fractal dimension and the power-law exponent of the population distribution. They also find that this distance exponent function can vary according to the population of origin and destination patches. In their work, they numerically validate their results and they have assumed that the location and population of each patch are fully uncorrelated with each other.

[40] shows how human mobility impacts the spread of infectious diseases between different set of patches (9 provinces, 25 districts and 339 divisional secretariats) in Sri Lanka, using multi-patch SIR model. They used several methods to collect mobility data, such as mobile phone data, which was collected in the form of aggregated and anonymized call data records of 17.7 million mobile subscribers across all coverage networks in 2021 from a leading telecommunications operator in Sri Lanka, Dialog Axiata. Moreover, they used data on the mobility of Face-

book application users in Sri Lanka was obtained from Meta's Facebook Disaster Map project. These data represented the movements of Facebook application users who opted into sharing their location history.

## 2.3 Objectives of the Research

In this work, study the more fundamental connection between the radiation and modified gravity models in a population landscape. In order to study such a connection first, consider a heterogeneous population landscape, which is the population of each patch following the power-law probability distribution. The radiation model on such population landscapes, namely, the radiation-on-landscape (RoL) model, can be written in terms of the distance between two patches. By expanding the rescaled travel probability in the RoL model and comparing it to the modified gravity model, derive the distance exponent in the modified gravity model as a function of properties of the population landscape. Also shows this distance exponent function can vary according to the population sizes of origin and destination patches. In our work, assume that the location and population of each patch are fully uncorrelated with each other.

Moreover, the radiation model is used to predict human mobility between provinces in Sri Lanka to overcome the complexity of studying human mobility and the lack of systematic mobility data. It is also connected with the multi-patch SIRD model to study how human mobility affects the spread of COVID-19 between provinces in Sri Lanka.

# Chapter 3

# Methodology

## Summary

This chapter explains the mathematical and computational techniques used in this study. In the first section, the distance exponent parameter in the modified gravity model will be derived as a function of properties of a population landscape. In the second section, the variables of the radiation model will be estimated and used to estimate human mobility between each province in Sri Lanka. The final section will develop the connection between the radiation model and the multi-patch SIRD model.

## 3.1 Connecting the Radiation-on-Landscape Model to the Modified Gravity Model

The connection between radiation and modified gravity models can be made by the observation in [10], that the surrounding population $s_{ij}$ of the radiation model in Equation 2.3 might be correlated with the distance $r_{ij}$ of the modified

gravity model in Equation 2.2. The relation between $s_{ij}$ and $r_{ij}$ can be analytically derive in population landscape model. Using this relation, the radiation model in population landscape, i.e., the radiation-on-landscape (RoL) model, can be described by Equation 2.3 but in terms of $r_{ij}$. By expanding the rescaled travel probability in the RoL model and comparing it to the modified gravity model, derive the distance exponent $\gamma$ as a function of properties of the population landscape. Also show this distance exponent function can vary according to the population sizes of origin and destination patches. In this work, assume that the location and population of each patch are fully uncorrelated with each other.

### 3.1.1 Scaling behavior of surrounding population

The surrounding population $s_{ij}$ of the radiation model as the total population, except for the patches, $i$ and $j$, within a circle centered at the patch $i$ with radius $r_{ij}$. Let denote by $A_{ij}$ the set of patches, except for $i$ and $j$, within a circle centered at the patch $i$ with radius $r_{ij}$, and the number of patches in $A_{ij}$ is denoted by $n_{ij}$. In a $d_f$ dimensional space, can write a relation between $n_{ij}$ and $r_{ij}$ below as [11]:

$$n_{ij} = c r_{ij}^{d_f} \tag{3.1}$$

with a coefficient $c > 0$. The surrounding population is defined as:

$$s_{ij} = \sum_{l \in \Lambda_{ij}} m_l = \sum_{k=1}^{n_{ij}} m_k \tag{3.2}$$

Where $m_k$ denotes the population of the $k$th populated site in $A_{ij}$ such that

$m_1 \geq m_2 \geq ... \geq m_{n_{ij}}$. As all $m_i$s are statistically independent of each other. There are $k$ patches in $A_{ij}$ such that $m_i \geq m_k$ here $i$ =1,2,...k, therefore, the probability of patches which $m_i \geq m_k$ in $A_{ij}$ gives as:

$$P(m_i \geq m_k) = \frac{k}{n_{ij}} = \int_{m_k}^{\infty} P(m)\, dm \tag{3.3}$$

$$\frac{k}{n_{ij}} = \int_{m_k}^{\infty} (\beta - 1)\, m_0^{\beta-1}\, m^{-\beta}\, dm \quad \text{here } \beta > 1$$

$$\frac{k}{n_{ij}} = (\beta - 1)\, m_0^{\beta-1} \int_{m_k}^{\infty} m^{-\beta}\, dm$$

$$\frac{k}{n_{ij}} = (\beta - 1)\, m_0^{\beta-1} \left[\frac{m^{1-\beta}}{1-\beta}\right]_{m_k}^{\infty} = (\beta - 1)\, m_0^{\beta-1} \frac{m_k^{1-\beta}}{\beta - 1}$$

$$m_k = m_0 \left(\frac{k}{n_{ij}}\right)^{-1/(\beta-1)} \tag{3.4}$$

From Equations 3.2,3.4, derive the surrounding population $s_{ij}$ in terms of $n_{ij}$ below as:

$$s_{ij} = \sum_{k=1}^{n_{ij}} m_k \approx \int_1^{n_{ij}} m_k\, dk$$

$$s_{ij} \approx \int_1^{n_{ij}} m_0 \left(\frac{k}{n_{ij}}\right)^{-1/(\beta-1)} dk \tag{3.5}$$

Consider, the below two cases of Equation 3.5 for different values of power-law exponent $\beta$.

Case (I): $\beta \neq 2$

$$s_{ij} \approx m_0 \left(\frac{1}{n_{ij}}\right)^{1/(1-\beta)} \int_1^{n_{ij}} k^{-1/(\beta-1)}\, dk = m_0 \left(\frac{1}{n_{ij}}\right)^{1/(1-\beta)} \left[\frac{k^{(\beta-2)/(\beta-1)}}{(\beta-2)/(\beta-1)}\right]_1^{n_{ij}}$$

$$s_{ij} \approx \frac{\beta-1}{\beta-2} m_0 \left(n_{ij} - n_{ij}^{1/(\beta-1)}\right)$$

Case (II): $\beta = 2$

$$s_{ij} \approx m_0 n_{ij} \int_1^{n_{ij}} \frac{1}{k}\, dk$$

$$s_{ij} \approx m_0 n_{ij} \ln n_{ij}$$

From Case (I) and Case (II), the surrounding population $s_{ij}$ below as:

$$s_{ij} \approx \begin{cases} \frac{\beta-1}{\beta-2} m_0 \left(n_{ij} - n_{ij}^{1/(\beta-1)}\right) & \text{for } \beta \neq 2 \\ m_0 n_{ij} \ln(n_{ij}) & \text{for } \beta = 2 \end{cases} \tag{3.6}$$

From Equations 3.1,3.6, rewrite the surrounding population $s_{ij}$ in terms of $r_{ij}$ below as:

$$s_{ij} \approx \begin{cases} \frac{\beta-1}{\beta-2} m_0 \left( c r_{ij}^{d_f} - c^{1/(\beta-1)} r_{ij}^{d_f/(\beta-1)} \right) & \text{for } \beta \neq 2 \\ m_0 c r_{ij}^{d_f} \ln(c r_{ij}^{d_f}) & \text{for } \beta = 2 \end{cases} \tag{3.7}$$

From Equation 3.7, the term of $r_{ij}^{d_f}$ dominates $s_{ij}$ for large $r_{ij}$ when $\beta \geq 2$. Moreover, the term of $r_{ij}^{d_f/(\beta-1)}$ dominates $s_{ij}$ for large $r_{ij}$ when $\beta < 2$. Therefore, $s_{ij}$ and $r_{ij}$ are asymptotically equivalent below as:

$$s_{ij} \sim r_{ij}^{\alpha} \tag{3.8}$$

with

$$\alpha = \begin{cases} d_f/(\beta-1) & \text{for } \beta < 2 \\ d_f & \text{for } \beta \geq 2 \end{cases} \tag{3.9}$$

### 3.1.2 Expansion of the RoL model

In this section, consider three cases of rescaled travel probability which discussed under Equation 2.5, such as : (I) $m_i, m_j \ll s_{ij}$, (II) $m_i \ll s_{ij} \ll m_j$, and (III) $s_{ij} \ll m_i$.

Case (I): $m_i, m_j \ll s_{ij}$

The denominator of rescaled travel probability is expanded as follows:

$$(m_i + s_{ij})(m_i + s_{ij} + m_j) = s_{ij}^2 \left(1 + \frac{m_i}{s_{ij}}\right) \left(1 + \frac{m_i + m_j}{s_{ij}}\right)$$

Moreover,

$$\frac{1}{\left(1+\frac{m_i+m_j}{s_{ij}}\right)} = \left(1 - \frac{m_i+m_j}{s_{ij}} + \mathcal{O}\left(\left(\frac{m_i+m_j}{s_{ij}}\right)^2\right)\right)$$

and

$$\frac{1}{\left(1+\frac{m_i}{s_{ij}}\right)} = \left(1 - \frac{m_i}{s_{ij}} + \mathcal{O}\left(\left(\frac{m_i}{s_{ij}}\right)^2\right)\right)$$

This allows the rescaled travel probability to be expanded as follows:

$$\frac{P_{ij}}{m_i m_j} = s_{ij}^{-2}\left(1 - \frac{m_i+m_j}{s_{ij}} + \mathcal{O}\left(\left(\frac{m_i+m_j}{s_{ij}}\right)^2\right)\right)\left(1 - \frac{m_i}{s_{ij}} + \mathcal{O}\left(\left(\frac{m_i}{s_{ij}}\right)^2\right)\right)$$

The term $\frac{m_i^2}{s_{ij}^2}$ dominates $\mathcal{O}\left(\left(\frac{m_i}{s_{ij}}\right)^2\right) = \sum_{n=2}^{\infty}(-1)^n\left(\frac{m_i}{s_{ij}}\right)^n$ therefore,

$$\sum_{n=1}^{\infty}\left(\frac{m_i}{s_{ij}}\right)^{2n+1} \ll \sum_{n=1}^{\infty}\left(\frac{m_i}{s_{ij}}\right)^{2n}$$

Furthermore, Without Loss of Generality (WLOG)

$$\mathcal{O}\left(\left(\frac{m_i}{s_{ij}}\right)^2\right) \approx \mathcal{O}\left(\frac{m_i^2}{s_{ij}^2}\right) = \sum_{n=1}^{\infty}\left(\frac{m_i}{s_{ij}}\right)^{2n}$$

Similarly,

$$\mathcal{O}\left(\left(\frac{m_i+m_j}{s_{ij}}\right)^2\right) \approx \mathcal{O}\left(\frac{m_i^2+2m_im_j+m_j^2}{s_{ij}^2}\right)$$

Since $m_i, m_j \ll s_{ij}$, it follows that $\left|\frac{m_i^2}{s_{ij}^2} - \frac{m_j^2}{s_{ij}^2}\right| \ll 1$ and $\left|\frac{m_i^2}{s_{ij}^2} - \frac{2m_im_j}{s_{ij}^2}\right| \ll 1$

WLOG

$$\mathcal{O}\left(\frac{m_i^2 + 2m_i m_j + m_j^2}{s_{ij}^2}\right) \approx \mathcal{O}\left(\frac{m_i^2}{s_{ij}^2}\right)$$

therefore, the rescaled travel probability as:

$$\frac{P_{ij}}{m_i m_j} \approx s_{ij}^{-2}\left(1 - \frac{m_i + m_j}{s_{ij}} + \mathcal{O}\left(\frac{m_i^2}{s_{ij}^2}\right)\right)\left(1 - \frac{m_i}{s_{ij}} + \mathcal{O}\left(\frac{m_i^2}{s_{ij}^2}\right)\right)$$

WLOG by omitting very small products of $\mathcal{O}\left(\frac{m_i^2}{s_{ij}^2}\right)$, gives rescaled travel probability below as:

$$\frac{P_{ij}}{m_i m_j} \approx s_{ij}^{-2}\left(1 - \frac{2m_i + m_j}{s_{ij}} + \frac{m_i m_j}{s_{ij}^2} + \frac{m_i^2}{s_{ij}^2} + \mathcal{O}\left(\frac{m_i^2}{s_{ij}^2}\right)\right)$$

Since $\left|\frac{m_i^2}{s_{ij}^2} - \frac{m_i m_j}{s_{ij}^2}\right| \ll 1$, WLOG it allows to rewrite the rescaled probability below as:

$$\frac{P_{ij}}{m_i m_j} \approx s_{ij}^{-2}\left(1 - \frac{2m_i + m_j}{s_{ij}} + \mathcal{O}\left(\frac{m_i^2}{s_{ij}^2}\right)\right) \tag{3.10}$$

Equation 3.8 and properties of asymptotically equivalent, allows to write $s_{ij}^{-2} \sim r_{ij}^{-2\alpha}$.Therefore, above asymptotically equivalent in Equation 3.8 provides the facility to describe Equation 3.10 in terms of $r_{ij}$ below as:

$$\frac{P_{ij}}{m_i m_j} \approx r_{ij}^{-2\alpha}\left(1 - \frac{2m_i + m_j}{r_{ij}^{\alpha}} + \mathcal{O}\left(\frac{m_i^2}{r_{ij}^{2\alpha}}\right)\right) \tag{3.11}$$

The term of $r_{ij}^{-2\alpha}$ dominates $\frac{P_{ij}}{m_i m_j}$ for $m_i, m_j \ll s_{ij}$ therefore, the new asymptotically equivalent below as:

$$\frac{P_{ij}}{m_i m_j} \sim r_{ij}^{-2\alpha} = \begin{cases} r_{ij}^{-2d_f/(\beta-1)} & \text{for } \beta < 2 \\ r_{ij}^{-2d_f} & \text{for } \beta \geq 2 \end{cases} \tag{3.12}$$

Furthermore, Equation 2.2 gives an asymptotically equivalent below as:

$$\frac{T_{ij}}{m_i m_j} \sim r_{ij}^{-\gamma} m_i^{\theta-1} m_j^{\omega-1} \tag{3.13}$$

and comparing Equations 3.12,3.13, the term $r_{ij}^{-2\alpha}$ does not depend on $m_i$ and $m_j$ therefore, $\theta = 1$ and $\omega = 1$ not only that

$$\gamma = 2\alpha = \begin{cases} 2d_f/(\beta-1) & \text{for } \beta < 2 \\ 2d_f & \text{for } \beta \geq 2 \end{cases} \tag{3.14}$$

Case (II): $m_i \ll s_{ij} \ll m_j$

The denominator of rescaled travel probability is expanded as:

$$(m_i + s_{ij})(m_i + s_{ij} + m_j) = s_{ij} m_j \left(1 + \frac{m_i}{s_{ij}}\right)\left(1 + \frac{m_i}{m_j} + \frac{s_{ij}}{m_j}\right)$$

Moreover,

$$\frac{1}{\left(1 + \frac{m_i}{s_{ij}}\right)} = \left(1 - \frac{m_i}{s_{ij}} + \mathcal{O}\left(\left(\frac{m_i}{s_{ij}}\right)^2\right)\right)$$

and

$$\frac{1}{\left(1 + \frac{m_i}{m_j} + \frac{s_{ij}}{m_j}\right)} = \left(1 - \frac{m_i}{m_j} - \frac{s_{ij}}{m_j} + \mathcal{O}\left(\left(\frac{m_i}{m_j} + \frac{s_{ij}}{m_j}\right)^2\right)\right)$$

It allows to expand the rescaled travel probability below as:

$$\frac{P_{ij}}{m_i m_j} = \frac{s_{ij}^{-1}}{m_j}\left(1 - \frac{m_i}{s_{ij}} + \mathcal{O}\left(\left(\frac{m_i}{s_{ij}}\right)^2\right)\right)\left(1 - \frac{m_i}{m_j} - \frac{s_{ij}}{m_j} + \mathcal{O}\left(\left(\frac{m_i}{m_j} + \frac{s_{ij}}{m_j}\right)^2\right)\right)$$

The term $\left(\frac{m_i}{m_j} + \frac{s_{ij}}{m_j}\right)^2$ dominates $\mathcal{O}\left(\left(\frac{m_i}{m_j} + \frac{s_{ij}}{m_j}\right)^2\right) = \sum_{n=2}^{\infty}(-1)^n\left(\frac{m_i}{m_j} + \frac{s_{ij}}{m_j}\right)^n$ therefore,

$$\sum_{n=1}^{\infty}\left(\frac{m_i}{m_j} + \frac{s_{ij}}{m_j}\right)^{2n+1} \ll \sum_{n=1}^{\infty}\left(\frac{m_i}{m_j} + \frac{s_{ij}}{m_j}\right)^{2n}$$

Furthermore, WLOG

$$\mathcal{O}\left(\left(\frac{m_i}{m_j} + \frac{s_{ij}}{m_j}\right)^2\right) \approx \mathcal{O}\left(\frac{m_i^2}{m_j^2} + \frac{2m_i s_{ij}}{m_j^2} + \frac{s_{ij}^2}{m_j^2}\right) = \sum_{n=1}^{\infty}\left(\frac{m_i}{m_j} + \frac{s_{ij}}{m_j}\right)^{2n}$$

Since $m_i \ll s_{ij} \ll m_j$, can take $\frac{m_i^2}{m_j^2} \approx 0$ and $\left|\frac{s_{ij}^2}{m_j^2} - \frac{2m_i s_{ij}}{m_j^2}\right| \ll 1$, WLOG

$$\mathcal{O}\left(\left(\frac{m_i}{m_j} + \frac{s_{ij}}{m_j}\right)^2\right) \approx \mathcal{O}\left(\frac{s_{ij}^2}{m_j^2}\right) = \sum_{n=1}^{\infty}\left(\frac{s_{ij}}{m_j}\right)^{2n}$$

Similarly, $\mathcal{O}\left(\left(\frac{m_i}{s_{ij}}\right)^2\right) \approx \mathcal{O}\left(\frac{m_i^2}{s_{ij}^2}\right)$ therefore, the rescaled travel probability as:

$$\frac{P_{ij}}{m_i m_j} \approx \frac{s_{ij}^{-1}}{m_j}\left(1 - \frac{m_i}{s_{ij}} + \mathcal{O}\left(\frac{m_i^2}{s_{ij}^2}\right)\right)\left(1 - \frac{m_i}{m_j} - \frac{s_{ij}}{m_j} + \mathcal{O}\left(\frac{s_{ij}^2}{m_j^2}\right)\right)$$

WLOG by omitting very small products of $\mathcal{O}\left(\frac{m_i^2}{s_{ij}^2}\right)$ and very small products of $\mathcal{O}\left(\frac{s_{ij}^2}{m_j^2}\right)$, the rescaled travel probability below as:

$$\frac{P_{ij}}{m_i m_j} \approx \frac{s_{ij}^{-1}}{m_j}\left(1+\frac{m_i^2}{m_j s_{ij}}-\frac{m_i}{s_{ij}}-\frac{s_{ij}}{m_j}+\mathcal{O}\left(\frac{m_i^2}{s_{ij}^2}\right)+\mathcal{O}\left(\frac{s_{ij}^2}{m_j^2}\right)\right)$$

Since $m_i \ll s_{ij} \ll m_j$, WLOG the products $\left(\frac{m_i^2}{s_{ij}^2}\right)^n \left(\frac{s_{ij}^2}{m_j^2}\right)^k \approx 0$ for $n, k \in \mathbb{N}$ therefore,

$$\mathcal{O}\left(\frac{m_i^2}{s_{ij}^2}\right)+\mathcal{O}\left(\frac{s_{ij}^2}{m_j^2}\right) \approx \mathcal{O}\left(\frac{m_i^2}{s_{ij}^2}+\frac{s_{ij}^2}{m_j^2}\right)$$

It allows to rewrite the rescaled travel probability below as:

$$\frac{P_{ij}}{m_i m_j} \approx \frac{s_{ij}^{-1}}{m_j}\left(1+\left(\frac{m_i^2}{m_j}-m_i\right)s_{ij}^{-1}-\frac{s_{ij}}{m_j}+\mathcal{O}\left(\frac{m_i^2}{s_{ij}^2}+\frac{s_{ij}^2}{m_j^2}\right)\right) \tag{3.15}$$

Equation 3.8) and properties of asymptotically equivalent, allows to write $s_{ij}^{-1} \sim r_{ij}^{-\alpha}$.Moreover, above asymptotically equivalent in Equation 3.8 provides the facility to describe Equation 3.15 in terms of $r_{ij}$ below as:

$$\frac{P_{ij}}{m_i m_j} \approx \frac{r_{ij}^{-\alpha}}{m_j}\left(1+\left(\frac{m_i^2}{m_j}-m_i\right)r_{ij}^{-\alpha}-\frac{r_{ij}^{\alpha}}{m_j}+\mathcal{O}\left(\frac{m_i^2}{r_{ij}^{2\alpha}}+\frac{r_{ij}^{2\alpha}}{m_j^2}\right)\right) \tag{3.16}$$

The term of $r_{ij}^{-\alpha} m_j^{-1}$ dominates $\frac{P_{ij}}{m_i m_j}$ for $m_i \ll s_{ij} \ll m_j$ therefore, the new asymptotically equivalent below as:

$$\frac{P_{ij}}{m_i m_j} \sim r_{ij}^{-\alpha} m_j^{-1} = \begin{cases} r_{ij}^{-d_f/(\beta-1)} m_j^{-1} & \text{for } \beta < 2 \\ r_{ij}^{-d_f} m_j^{-1} & \text{for } \beta \geq 2 \end{cases} \tag{3.17}$$

and comparing Equations 3.13,3.17, the term $r_{ij}^{-\alpha} m_j^{-1}$ does not depend on

$m_i$ therefore, $\theta = 1$ not only that by properties of asymptotically equivalent $m_j^{-1} r_{ij}^{-\alpha} \sim r_{ij}^{-\gamma} m_j^{\omega-1}$ and $m_j^{-\omega} r_{ij}^{-\alpha} \sim r_{ij}^{-\gamma}$. Moreover, $-\omega\alpha \log(m_j) - \alpha \log(r_{ij}^{\alpha}) \sim -\gamma \log(r_{ij}^{\alpha})$ here $\lim_{r_{ij}\to\infty} r_{ij}^{\alpha} \neq 1$. Since $m_i \ll s_{ij} \ll m_j$, from Equation 3.8, can say $\log(m_i) < \log(r_{ij}^{\alpha}) \neq 0$ then the distance exponent $\gamma$ below as:

$$\gamma = \alpha \left(1 + \omega \frac{\log(m_j)}{\log(r_{ij}^{\alpha})}\right) \tag{3.18}$$

with

$$\alpha = \begin{cases} d_f/(\beta - 1) & \text{for } \beta < 2 \\ d_f & \text{for } \beta \geq 2 \end{cases}$$

Case (III): $s_{ij} \ll m_i, m_j$

The denominator of rescaled travel probability is expanded as:

$$(m_i + s_{ij})(m_i + s_{ij} + m_j) = m_i(m_i + m_j)\left(1 + \frac{s_{ij}}{m_i}\right)\left(1 + \frac{s_{ij}}{m_i + m_j}\right)$$

Moreover,

$$\frac{1}{\left(1 + \frac{s_{ij}}{m_i}\right)} = \left(1 - \frac{s_{ij}}{m_i} + \mathcal{O}\left(\left(\frac{s_{ij}}{m_i}\right)^2\right)\right)$$

and

$$\frac{1}{\left(1 + \frac{s_{ij}}{m_i + m_j}\right)} = \left(1 - \frac{s_{ij}}{m_i + m_j} + \mathcal{O}\left(\left(\frac{s_{ij}}{m_i + m_j}\right)^2\right)\right)$$

It allows to expand the rescaled travel probability below as:

$$\frac{P_{ij}}{m_i m_j} = \frac{1}{m_i(m_i+m_j)}\left(1-\frac{s_{ij}}{m_i}+\mathcal{O}\left(\left(\frac{s_{ij}}{m_i}\right)^2\right)\right)\left(1-\frac{s_{ij}}{m_i+m_j}+\mathcal{O}\left(\left(\frac{s_{ij}}{m_i+m_j}\right)^2\right)\right)$$

The term $\left(\frac{s_{ij}}{m_i+m_j}\right)^2$ dominates $\mathcal{O}\left(\left(\frac{s_{ij}}{m_i+m_j}\right)^2\right) = \sum_{n=2}^{\infty}(-1)^2\left(\frac{s_{ij}}{m_i+m_j}\right)^n$ therefore,

$$\sum_{n=1}^{\infty}\left(\frac{s_{ij}}{m_i+m_j}\right)^{2n+1} \ll \sum_{n=1}^{\infty}\left(\frac{s_{ij}}{m_i+m_j}\right)^{2n}$$

Furthermore, WLOG

$$\mathcal{O}\left(\left(\frac{s_{ij}}{m_i+m_j}\right)^2\right) \approx \mathcal{O}\left(\frac{s_{ij}^2}{m_i^2+2m_im_j+m_j^2}\right) = \sum_{n=1}^{\infty}\left(\frac{s_{ij}}{m_i+m_j}\right)^{2n}$$

Since $s_{ij} \ll m_i, m_j$, it follows that $\left|\left(\frac{s_{ij}}{m_i+m_j}\right)^{2n} - \left(\frac{s_{ij}}{2m_i}\right)^{2n}\right| \ll 1$ for $n \in \mathbb{N}$, WLOG

$$\mathcal{O}\left(\left(\frac{s_{ij}}{m_i+m_j}\right)^2\right) \approx \mathcal{O}\left(\frac{s_{ij}^2}{m_i^2}\right) = \sum_{n=1}^{\infty}\left(\frac{s_{ij}}{m_i}\right)^{2n}$$

Similarly, $\mathcal{O}\left(\left(\frac{s_{ij}}{m_i}\right)^2\right) \approx \mathcal{O}\left(\frac{s_{ij}^2}{m_i^2}\right)$ therefore, the rescaled travel probability below as:

$$\frac{P_{ij}}{m_i m_j} \approx \frac{1}{m_i(m_i+m_j)}\left(1-\frac{s_{ij}}{m_i}+\mathcal{O}\left(\frac{s_{ij}^2}{m_i^2}\right)\right)\left(1-\frac{s_{ij}}{m_i+m_j}+\mathcal{O}\left(\frac{s_{ij}^2}{m_i^2}\right)\right)$$

WLOG by omitting very small products of $\mathcal{O}\left(\frac{s_{ij}^2}{m_i^2}\right)$, the rescaled travel prob-

ability below as:

$$\frac{P_{ij}}{m_i m_j} \approx \frac{1}{m_i(m_i+m_j)}\left(1-\frac{s_{ij}}{m_i}-\frac{s_{ij}}{m_i+m_j}+\frac{s_{ij}^2}{m_i(m_i+m_j)}+\mathcal{O}\left(\frac{s_{ij}^2}{m_i^2}\right)\right)$$

Since $s_{ij} \ll m_i, m_j$, it follows that $\left|\frac{s_{ij}^2}{2m_i^2}-\frac{s_{ij}^2}{m_i(m_i+m_j)}\right| \ll 1$ therefore, WLOG the rescaled travel probability below as:

$$\frac{P_{ij}}{m_i m_j} \approx \frac{1}{m_i(m_i+m_j)}\left(1-\frac{2m_i+m_j}{m_i(m_i+m_j)}s_{ij}+\mathcal{O}\left(\frac{s_{ij}^2}{m_i^2}\right)\right) \tag{3.19}$$

The term of $\frac{1}{m_i(m_i+m_j)}$ dominates $\frac{P_{ij}}{m_i m_j}$ for $s_{ij} \ll m_i, m_j$ therefore, the new asymptotically equivalent below as:

$$\frac{P_{ij}}{m_i m_j} \sim \frac{1}{m_i(m_i+m_j)} \tag{3.20}$$

and comparing Equations 3.13,3.20 the term $\frac{1}{m_i(m_i+m_j)}$ does not depend on $r_{ij}$ therefore, the distance exponent

$$\gamma = 0. \tag{3.21}$$

The above analysis shows, the distance exponent $\gamma$ in modified gravity model as a function of the fractal dimension $d_f$ and the power-law exponent $\beta$ of the population distribution, the potential to attract movement $\omega$ of the modified gravity model and the distance $r_{ij}$ between origin $i$ and destination $j$ patches. Moreover, it shows this distance exponent function can vary according to the population of origin $m_i$ and destination $m_i$ patches such as Equations 3.14,3.18,3.21. This strongly implies that a given data set does not necessarily have to be character-

ized by the single value of the distance exponent, and it depends on the properties of the population landscape.

## 3.2 Understanding Human Mobility Patterns Between Provinces

This section studies human mobility patterns between provinces in Sri Lanka using the finite version of the radiation model. The radiation model Equation 2.3 has been derived in the thermodynamic limit, that is for an infinite system. It is easy to show that for a finite system the normalization brings us to a slightly different form of the radiation model [41], given by:

$$T_{ij} = T_i \frac{m_i m_j}{(1 - \frac{m_i}{M})(m_i + s_{ij})(m_i + m_j + s_{ij})} \tag{3.22}$$

Where $T_{ij}$ is the the average human flow (average number of commuters) from patch $i$ (origin) to patch $j$ (destination), $T_i \equiv \sum_{j \neq i} T_{ij}$ is the total number of commuters that start their journey from patch $i$, $M$ is the total population, $m_i$ is the population of patch $i$, $m_j$ is the population of patch $j$, $s_{ij}$ is the total population in the circle of radius $r_{ij}$ centered at patch $i$ excluding the population of patch $i$ and patch $j$.

### 3.2.1 Define the center of provinces

Equation 3.22 includes the surrounding population term $s_{ij}$ therefore, it is necessary to estimate $s_{ij}$ before studying human mobility between provinces. Moreover, according to the definition of $s_{ij}$, it refers to the population surrounding the cen-

ter of province $i$. This highlights the importance of defining the center of each province.

There are several methods to define a suitable center for a province. In this study, a data format known as **Raster** is used as the key tool for identifying an appropriate center for each province. The raster is a type of spatial data format used in GIS (Geographic Information Systems) to represent geographic information as a grid of pixels (cells). Each pixel in the raster has a value that represents information such as elevation, temperature, land cover, population density, etc. According to the context, the population-weighted centroid is considered the center of a province. The following reasons support this choice:

1. Population-weighted centroid is pulled towards areas with more people, which means it better represents where human activities are centered.

2. The first reason helps to ensure that flows start/end in places where people are actually located. It improving model performance and reducing errors.

Based on the above choice, the **Raster** data format should be selected, where each pixel contains a value representing population density information.

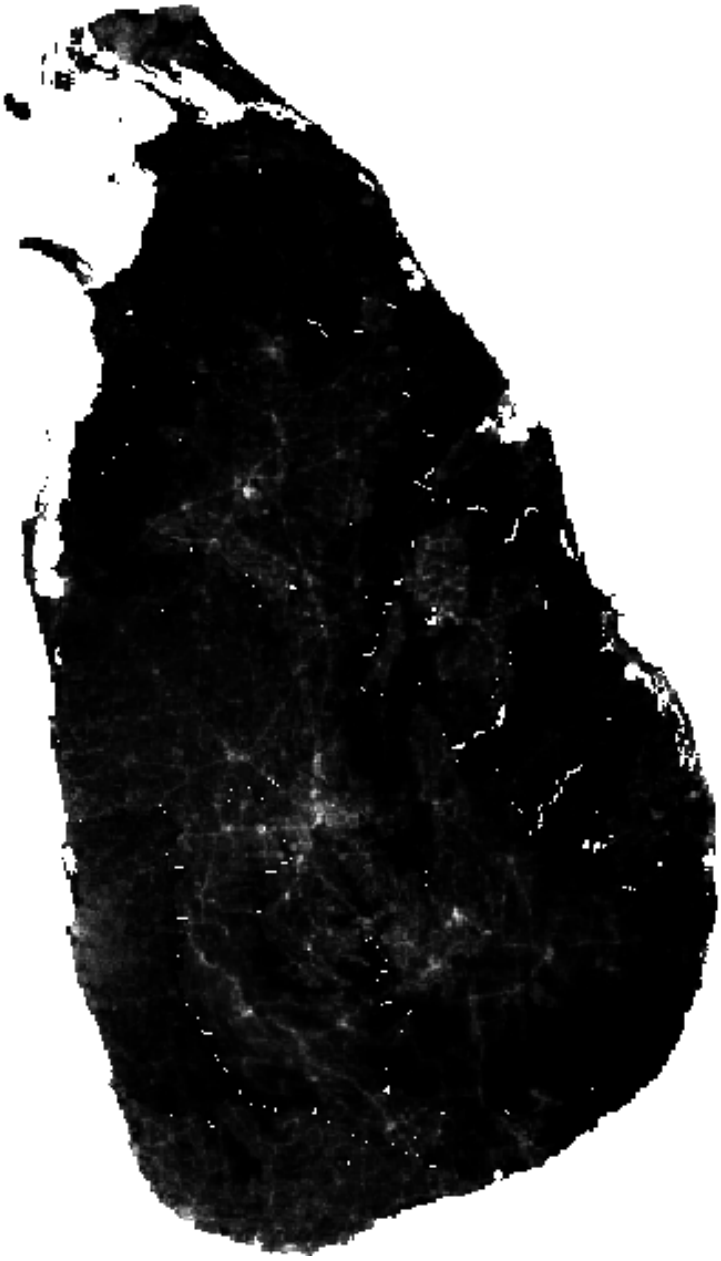

Figure 3.1: Population density in 2020 in Sri Lanka which generated by the raster data format.

The Figure 3.1 shows the population density in 2020 in Sri Lanka, which was generated by the raster data format. Moreover, the land of Sri Lanka is divided into pixels (one-square-kilometer boxes) and their intensity is used to represent

population density. The intensity of a pixel ranges from darker (lower population densities) to whiter (higher population densities).

Figure 3.2: The boundaries of each district in Sri Lanka.

The software called **QGIS** (Quantum Geographic Information System) used to select individual provinces and mark their boundaries from Figure 3.2. QGIS

is a free, open-source software that allows users to create, edit, visualize, analyze, and publish geospatial information. There are many benefits to using QGIS such as the software offers many free online resources and maps available to download and QGIS accepts many vector file formats.

First, import the shapefile of Figure 3.2 to the QGIS and choose the function called **Select Feature(s)** to select each district of a province. After that, choose the function **vector** → **Geoprocessing Tools** → **Dissolve**, active **Selected features only** option and click **Run**. After following the above steps for each province, the provinces and their boundaries are shown below:

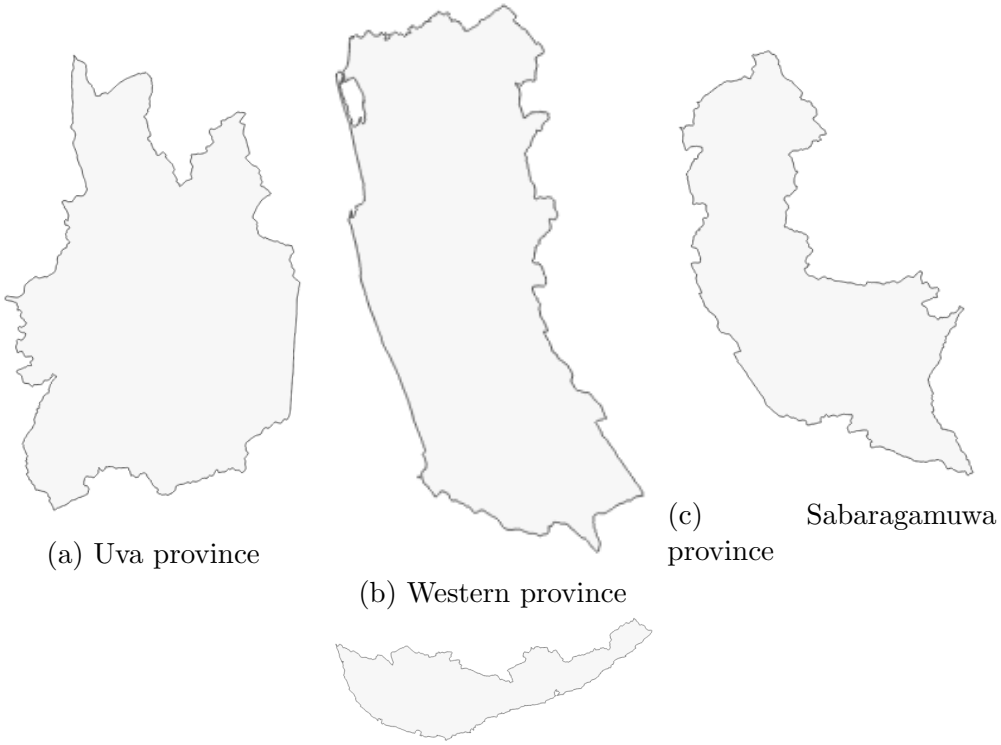

(a) Uva province

(b) Western province

(c) Sabaragamuwa province

(d) Southern province

Figure 3.3: Uva, Western, Sabaragamuwa and Southern provinces and their boundaries separately.

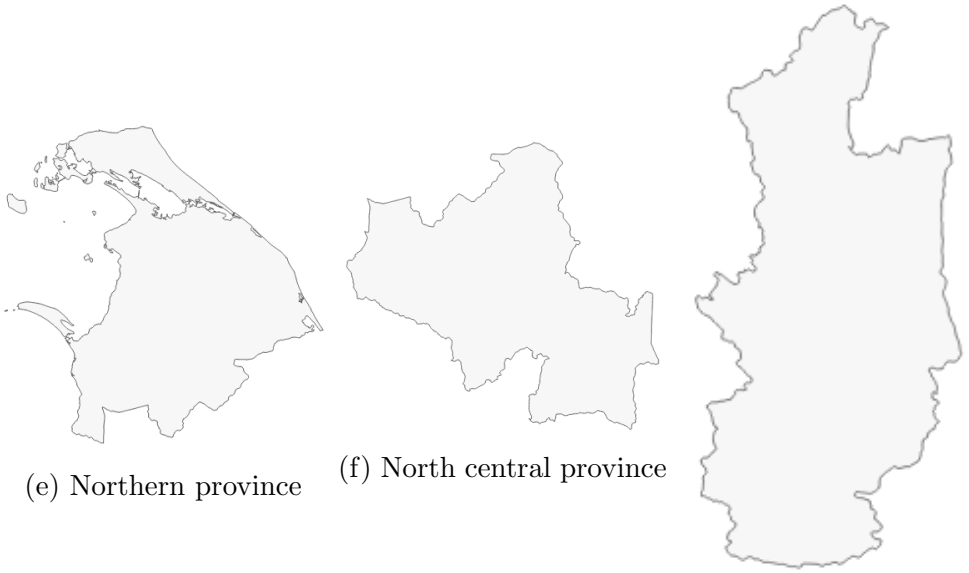

(e) Northern province

(f) North central province

(g) Central province

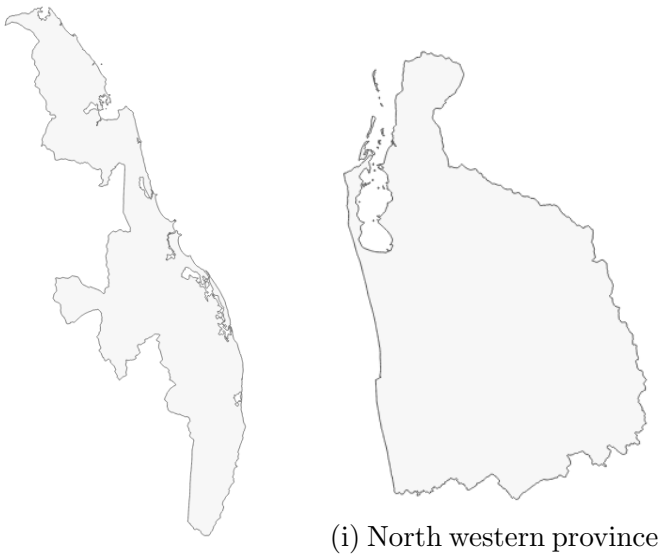

(h) Eastern province

(i) North western province

Figure 3.4: Northern, North central, Central, Eastern and North western provinces and their boundaries separately.

Now, select the shapefile of a province which created above and the population density map, which discussed in Figure 3.1, in QGIS. After that, search and select the function called **Clip Raster by Mask Layer** on **Processing Toolbox**,

then select the population density map for **Input layer**, select the shapefile of the province for **Mask layer**, select the option called **Mask layer extent** and **Run**. Similarly, by following the above steps for each province, a population density map for each province will be created, as shown below:

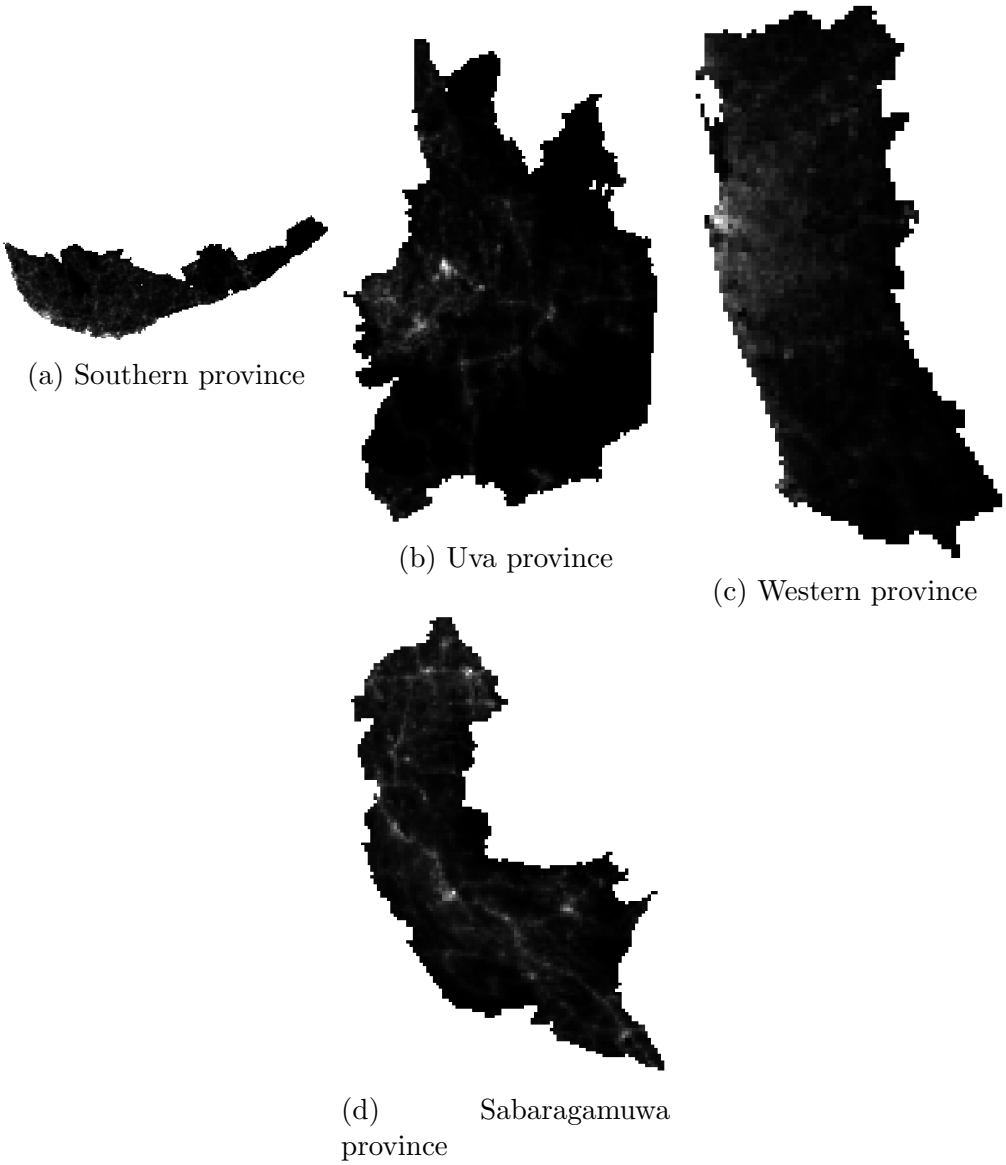

(a) Southern province

(b) Uva province

(c) Western province

(d) Sabaragamuwa province

Figure 3.5: The population density map of Southern, Uva, Western and Sabaragamuwa provinces, which was generated by the raster data format.

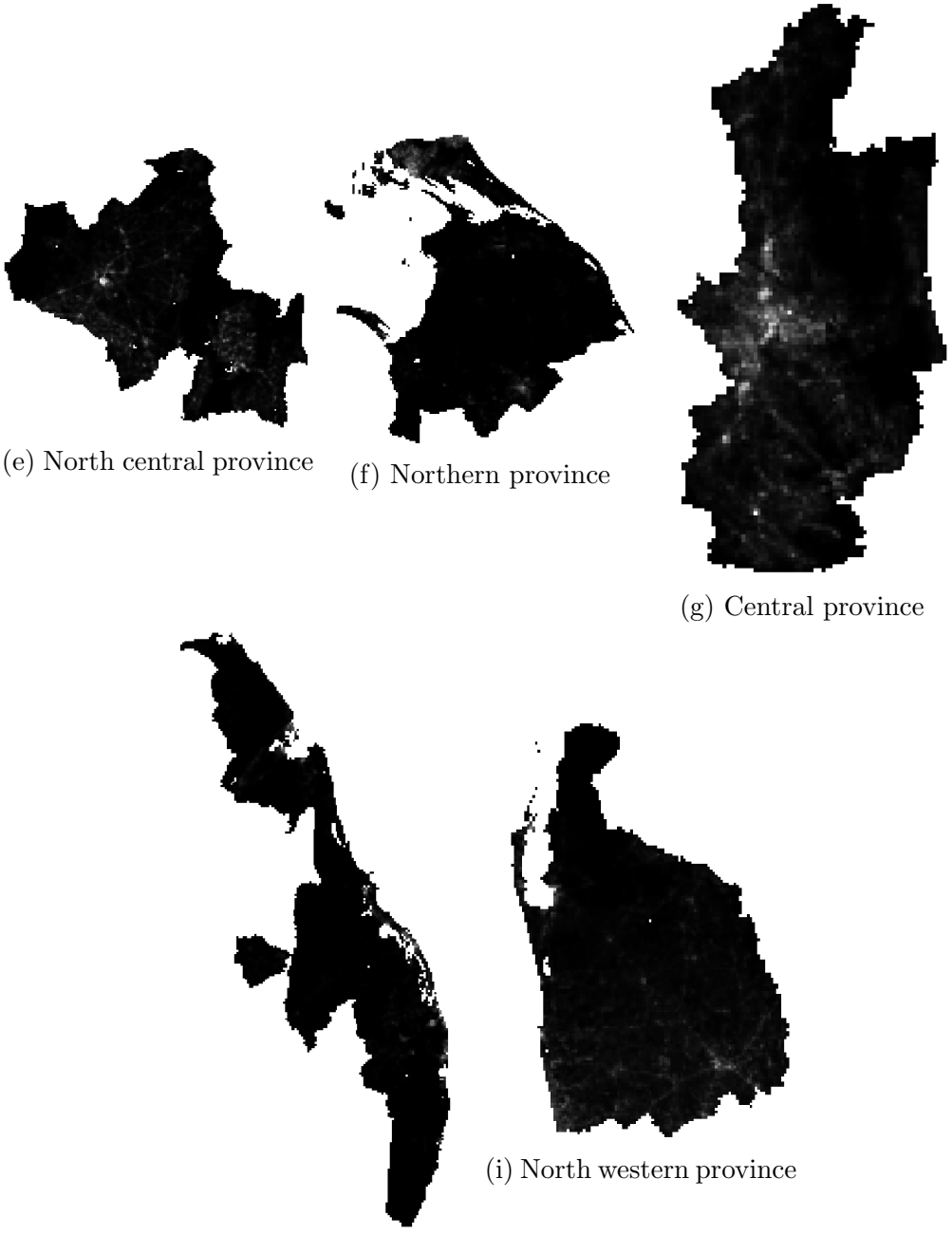

(e) North central province (f) Northern province

(g) Central province

(h) Eastern province (i) North western province

Figure 3.6: The population density map of North central, Northern, Central, Eastern and North western provinces, which was generated by the raster data format.

Further, QGIS is used to assign a population for each pixel corresponding to

its intensity. Moreover, this population represent by a fixed point in corresponding one-square-kilometer box (pixel) with geographic coordinate system WGS84 (World Geodetic System 1984). WGS84 is a globally standardized coordinate system used to define positions on Earth's surface, most commonly used in GPS navigation and mapping applications. The above population assigning process is shown in the following steps.

From the **Processing Toolbox**, search and select the function called **Vector creation** → **Raster pixels to points** then select the population density map of a province for **Raster layer**, type the filed name as `"population"` on **Field name** text box and **Run**. The filed `"population"` is used to save the population of each one-square-kilometer box (pixel) of the province. Similarly, by following the above steps for each province, the entire population of each province will be distributed by fixed points below as:

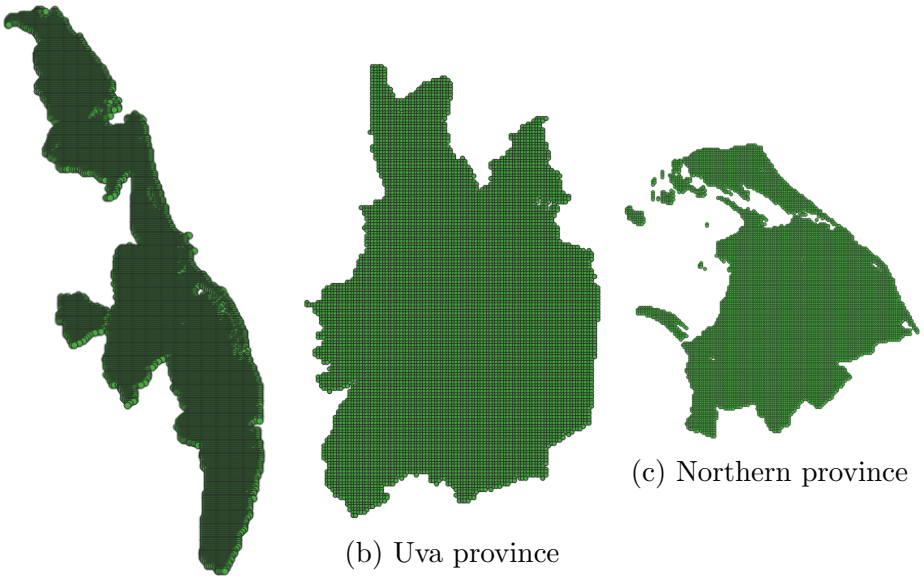

(a) Eastern province

(b) Uva province

(c) Northern province

Figure 3.7: Assigning a population by fixed point for each one-square-kilometer box (pixel) of Eastern, Uva and Northern provinces corresponding to pixel intensity.

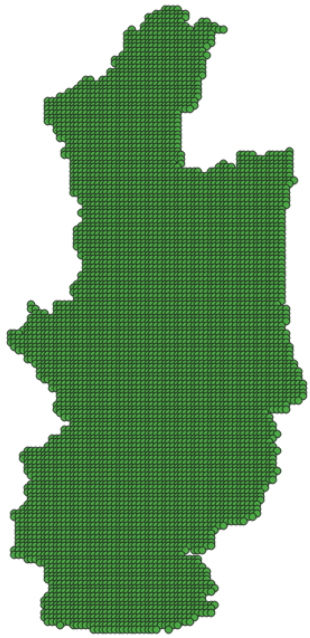

(d) Central province

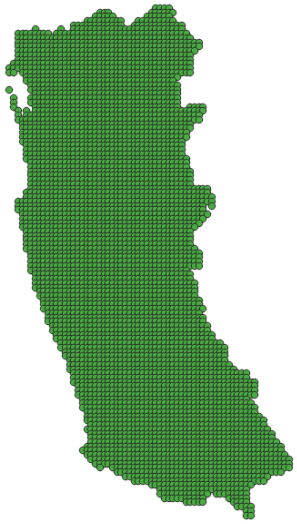

(e) Western province

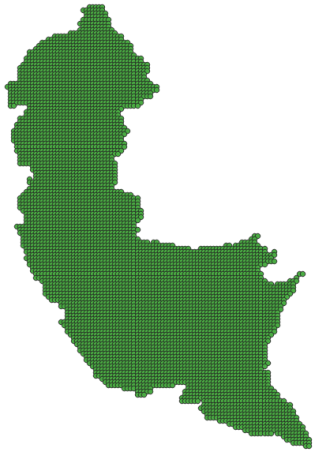

(f) Sabaragamuwa province

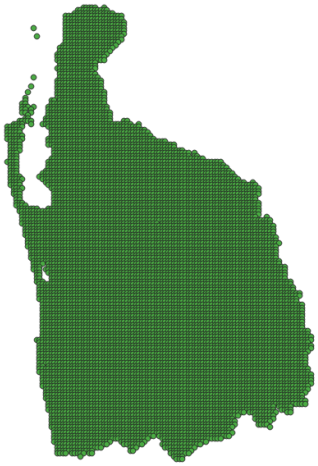

(g) North western province

(h) Southern province

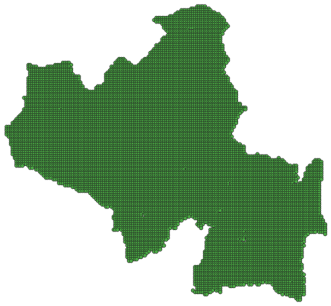

(i) North central province

Figure 3.8: Assigning a population by fixed point for each one-square-kilometer box (pixel) of Central, Western, Sabaragamuwa, North western, Southern and North central provinces corresponding to pixel intensity.

The latitude and longitude of the population-weighted centroid of a province calculated below as:

$$y_{latitude} = \frac{\sum y_i w_i}{\sum w_i} \tag{3.23}$$

$$x_{longitude} = \frac{\sum x_i w_i}{\sum w_i} \tag{3.24}$$

here $y_i$ is the latitude and $x_i$ is the longitude of the $i^{th}$ fixed point which used to represent the population $w_i$ of the $i^{th}$ one-square-kilometer box (pixel) of the province. The above concept is used in QGIS to find the population-weighted centroid of a province, and the steps are shown below.

First, select the layer of a province, which discussed in Figure 3.7,3.8. After that, using **Processing Toolbox**, search and select the function called **Vector analysis** → **Mean Coordinate(s)** then select the `"population"` for **Weight field** [**optional**] and **Run**. Similarly, by following the above steps for each province then, defined population-weighted centroids shown by below table.

| Index | Province name | Latitude | Longitude |
|---|---|---|---|
| 1 | Central | 7.257623555216736 | 80.6552744508472 |
| 2 | Eastern | 7.760791876319797 | 81.53477289343509 |
| 3 | North central | 8.187771264730436 | 80.65926156763892 |
| 4 | North western | 7.620874508038363 | 80.12462415445006 |
| 5 | Northern | 9.432459745567076 | 80.1728403332675 |
| 6 | Sabaragamuwa | 6.845243568262474 | 80.45120737257064 |
| 7 | Southern | 6.144353859524218 | 80.49751857194683 |
| 8 | Uva | 6.919277052291847 | 81.09719733888063 |
| 9 | Western | 6.905776795482587 | 79.97393595090782 |

Table 3.1: The latitude and longitude of the population-weighted centroid of each province in geographic coordinate system WGS84.

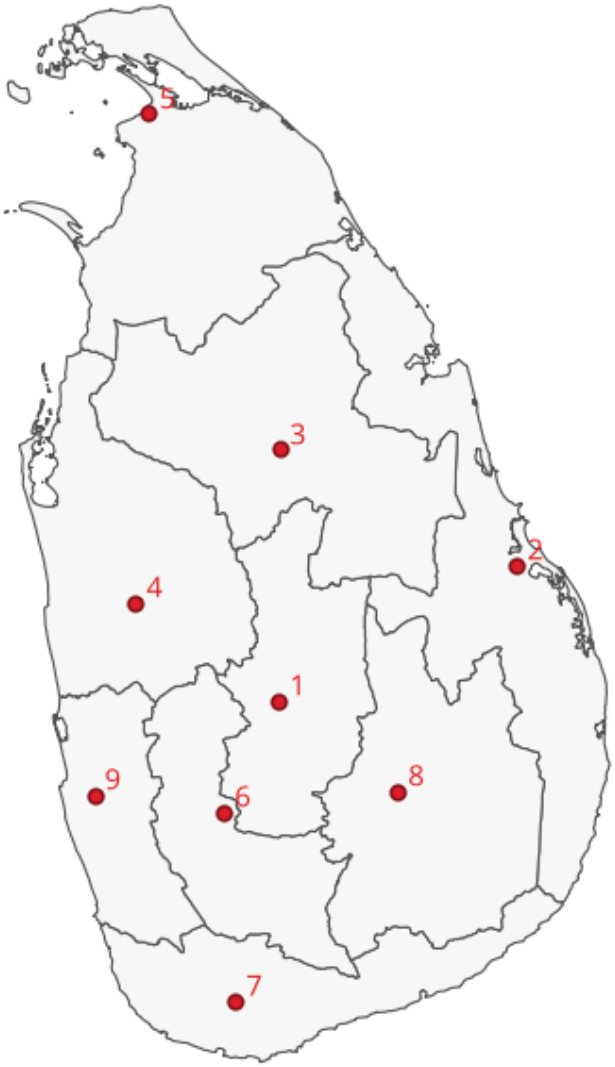


Figure 3.9: The population-weighted centroid for each province.

### 3.2.2 Estimate surrounding populations

The surrounding population $s_{ij}$ is the total population in the circle of radius $r_{ij}$ centered at province $i$ excluding the population of province $i$ and province $j$. According to the definition of $s_{ij}$, the population of the provinces and the distance $r_{ij}$ between province $i$ and province $j$ must be know.

The population of each province in Sri Lanka for the year 2020 is shown in the Table 3.2.

| Index | Province name | Population (in thousands) |
|---|---|---|
| 1 | Central | 2781 |
| 2 | Eastern | 1746 |
| 3 | North central | 1386 |
| 4 | North western | 2563 |
| 5 | Northern | 1152 |
| 6 | Sabaragamuwa | 2070 |
| 7 | Southern | 2669 |
| 8 | Uva | 1387 |
| 9 | Western | 6165 |

Table 3.2: This table shows the population of each province in 2020.

The following steps in QGIS are used to find the distance between provinces.

Step 1: Select the function called **Vector** → **Data Management Tools** → **Marge Vector Layers** then select every population-weighted centroid for **Input layers**, select the WGS84 coordinate system for **Destination CRD** [**optional**] and **Run**. The objective of Step 1 is to combine every population-weighted centroid into a single layer called `"Weighted centroids"`.

Step 2: Select the function called **Vector** → **Analysis Tools** → **Distance Matrix** then select the layer `"Weighted centroids"` which created in Step 1 for **Input point layer**, select the layer `"Weighted centroids"` for **Target point layer** and **Run**.

The distances between provinces, obtained from the above steps, are graphically represented in the heatmap below.

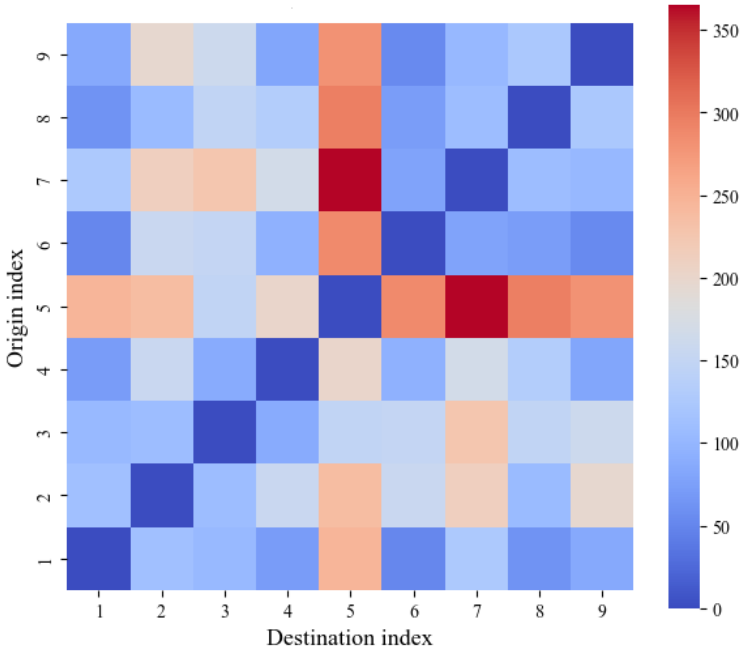


Figure 3.10: Heatmap of the distance between provinces.

The Figure 3.10 shows the heatmap of the distance between provinces in kilometers for each pair of provinces with their index. Moreover, the intensity of each pixel goes from blue color to red color when the distance increases.

The distances between provinces, obtained from the above steps, along with the population data from Table 3.2, allow for the calculation of the surrounding population for each pair of provinces. The example below illustrates the method of determining the surrounding population based on its definition.

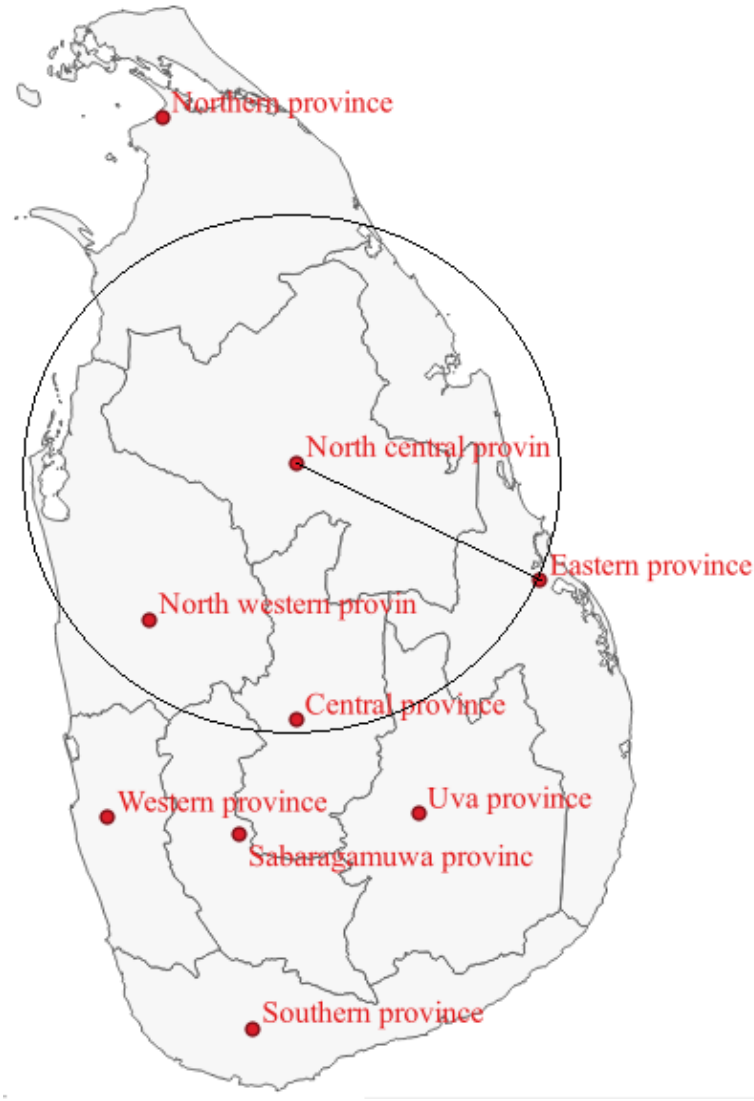


Figure 3.11: An example of a graphical representation for determining the surrounding population.

The Figure 3.11 shows an example graphical representation of the surrounding population, whose origin is the North central province and destination is the Eastern province. According to this, the surrounding population of North central province is the summation of the population of North western and Central provinces i.e, 2563000 + 2781000 = 5344000.

The surrounding populations, calculated for each pair of provinces as shown in the above example, are graphically represented in the heatmap below.

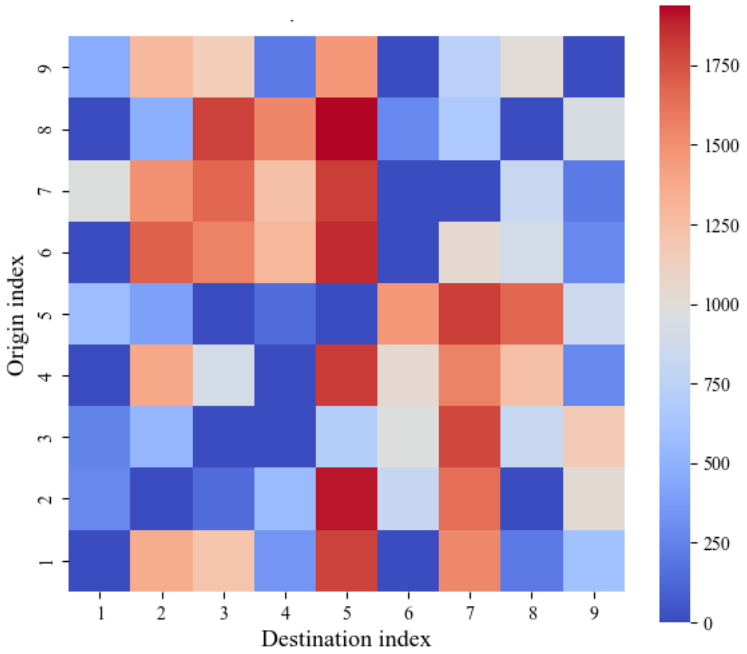


Figure 3.12: Heatmap of the surrounding population

The Figure 3.12 shows the heatmap of the surrounding population in ten thousands for each pair of provinces with their index. Moreover, the intensity of each pixel goes from blue color to red color when the surrounding population increases.

The distances between provinces and the surrounding population values for each pair of provinces are shown in Tables A.1-A.9.

### 3.2.3 Estimate human mobility between provinces

The Equation 3.22 use to define the travel probability from province $i$ to province $j$ for a finite system,as shown below:

$$P_{ij}^{*} = \frac{T_{ij}}{T_i} = \frac{m_i m_j}{(1 - \frac{m_i}{M})(m_i + s_{ij})(m_i + m_j + s_{ij})} \tag{3.25}$$

The population of each province in Table 3.2, the surrounding population $s_{ij}$ for each pair of provinces in Tables A.1-A.9 and the total population $M$ = 21,919,000 in Sri Lanka for the year 2020. The travel probability for the finite system $P_{ij}^{*}$ is given by $T_{ij}/T_i$ with $T_i \equiv \sum_{j \neq i} T_{ij}$ therefor, the Equation 3.25 doesn't satisfy the stochastic property, i.e, $\sum_{j=1}^{j=9} P_{ij}^{*} \neq 1$ for $i$ = 1,2,..,9. According to the stochastic property, normalize the values $P_{ij}^{*}$ as $P_{ij}^{*} / \sum_{j=1}^{j=9} P_{ij}^{*}$ for each pair of provinces.

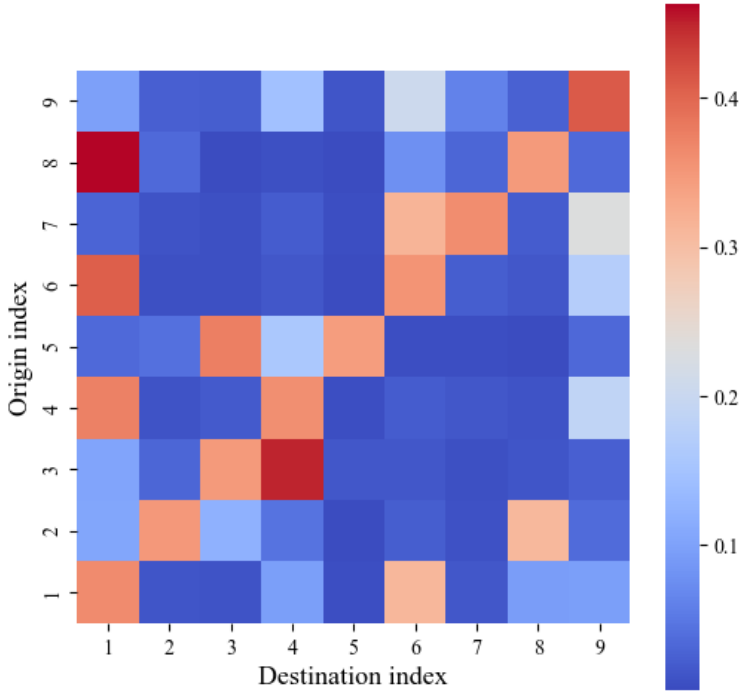


Figure 3.13: Heatmap of the normalized travel probability for the finite system.

The Figure 3.13 shows the heatmap of the normalized travel probability for the finite system, with their index. Moreover, the intensity of each pixel goes from blue color to red color when the normalized travel probability increases.

Moreover, the travel probability for the finite system $P_{ij}^{*}$ and their normalized values for each pair of provinces are shown in the Tables A.10-A.18.

## 3.3 Connecting Human Mobility Data With Multi-Patch SIRD Model

The connection between human mobility data with the multi-patch SIRD model can be developed by the term $W_{ij}$ in the multi-patch SIRD model, which discussed before. According to the definition, $W_{ij}$ is the proportion of individuals from province $i$ who are currently in province $j$. Moreover, the Equation 3.25 and $T_i = m_i(M_c/M)$ allows to define $W_{ij}$ below as:

$$W_{ij} = \frac{T_{ij}}{m_i} = \frac{M_c}{M} \frac{m_i m_j}{(1 - \frac{m_i}{M})(m_i + s_{ij})(m_i + s_{ij} + m_j)} \tag{3.26}$$

here $M_c$ is the total commuters per day.

| Passengers | 2017 | 2018 | 2019 |
|---|---|---|---|
| Railway | 136663 | 137524 | 128476 |
| Ominibus services | 2940413 | 3233443 | 3159088 |
| Sri Lanka transport board | 1005205 | 952778 | 916964 |
| Sri Lanaka airlines | 5361 | 5882 | 5579 |
| Foreign airlines | 4559 | 4917 | 4321 |
| Total | 4092198 | 4334544 | 4214428 |

Table 3.3: The number of commuters in thousands in 2017, 2018, and 2019 for different travel sources.

According to the Table 3.3, the average total commuters per day $M_c$ below as:

$$M_c = 1000\frac{(4092198 + 4334544 + 4214428)}{1095} = 1000\frac{12641170}{1095} \approx 11544447$$

The proportion of individuals from province $i$ who are currently in province $j$ i.e., $W_{ij}$ doesn't satisfy the stochastic property, i.e, $\sum_{j=1}^{j=9} W_{ij} \neq 1$ for $i$ = 1,2,..,9 because, every individuals in province $i$ are not commuters. According to the stochastic property, normalize $W_{ij}$ as $W_{ij}/\sum_{j=1}^{j=9} W_{ij}$ for each pair of provinces.

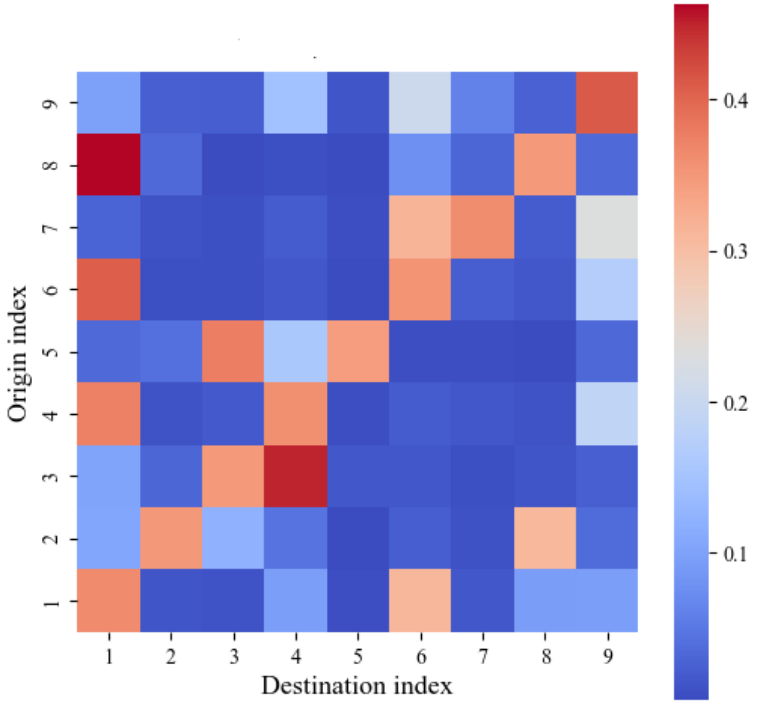


Figure 3.14: Heatmap of the normalized values of proportion of individuals from one province who are currently in another province.

The Figure 3.14 shows the normalized proportion of individuals from province $i$ who are currently in province $j$ for each $i$,$j \in$ {1,2,..,9}. The intensity of each pixel goes from blue color to red color when the normalized $W_{ij}$ increases.

Moreover, the proportion of individuals from province $i$ who are currently in province $j$ i.e., $W_{ij}$ and their normalized values for each pair of provinces are shown in the Tables A.19-A.27.

# Chapter 4

# Experimental Results

## Summary

Chapter 4 presents the overview of COVID-19 in Sri Lanka, parameter values and initial conditions of the multi-patch SIRD model based on the COVID-19 context. Moreover, the last section of this chapter contains the results of the multi-patch SIRD model, which is connected to the radiation model in the last section of Chapter 3, and these results show the spread of COVID-19 between provinces in Sri Lanka.

## 4.1 Overview of COVID-19 in Sri Lanka

COVID-19 is caused by a new coronavirus (SARS CoV-2) that emerged in China in December 2019 [42]. Most people who get infected with the virus either have no symptoms or only mild illness. However, in some cases, the infection can become very serious, affecting the lungs and making it hard to breathe or even leading to death. Transmission is mainly via droplets released into the air when an infected person coughs or sneezes. There is no vaccine at the earlier stage of

the virus thus, traditional measures that control the spread of infectious diseases such as quarantine, contact tracing, isolation of positives and contacts as well as social distancing and hand-washing are of vital importance.

The basic reproductive number $R_0$ is defined as the expected number of secondary infections arising from a single individual during his or her entire infectious period in a susceptible population. This concept is fundamental to the study of epidemiology and within-host pathogen dynamics. Most importantly, $R_0$ often serves as a threshold parameter that predicts whether an infection will spread [43].

The 1st case of COVID-19 was diagnosed in Sri Lanka on 27 January 2020, by a tourist from China. The 2nd case was detected nearly 6 weeks later, on 11 March, by a tour guide who probably contracted the infection from Italian tourists. After the second case, the virus spread slowly and mainly affected people who came from countries with many COVID-19 cases and the people who had close contact with them. However, it must be noted that in four of the 190 cases diagnosed in the 30 days from 11 March to 10 April 2020, it was not possible to identify the source of infection. Moreover, the number of COVID-19 cases doubled from 50 to 100 in about a week (from March 19 to March 25). However, after that, the number of cases grew more slowly because, by April 11, the total was 197 cases instead of doubling to 200 or more. By this date, 54 people had recovered, and 7 people had died [42].

The Sri Lankan government responded quickly to control the spread of COVID-19 by using strict health and safety measures. These included the complete country-wide lockdown, tracking and isolating infected people and their contacts, and quarantining all travellers entering the country. All these actions were taken at the same time to prevent further infections. The airport has been closed for

inbound passengers since 19 March [42]. Sri Lanka's official policy for COVID-19 testing was to test only people who showed symptoms and were clinically suspected of having the virus. The tests were conducted in seven specific laboratories using the PCR test, which is a reliable method to detect the virus. All infected individuals are managed in one of three state hospitals, designated for management of COVID-19. These hospitals are also equipped with intensive care units and ventilators for the management of the critically ill.

## 4.2 Parameter Values and Initial Conditions of Multi-Patch SIRD Model

The system of differential equations, discussed in the multi-patch SIRD model section, is shown below.

$$\frac{d}{dt}S_i(t) = -S_i(t)\sigma_i$$

$$\frac{d}{dt}I_i(t) = S_i(t)\sigma_i - \alpha_i I_i(t) - \mu I_i(t)$$

$$\frac{d}{dt}R_i(t) = \alpha_i I_i(t)$$

$$\frac{d}{dt}D_i(t) = \mu I_i(t)$$

where $S_i(t)$, $I_i(t)$, $R_i(t)$ and $D_i(t)$ denote the population of susceptible, infected, recovered and disease-induced death individuals respectively, in patch $i$ in period $t$. The parameters $\alpha_i$ denotes the per-capita recovery rate in patch $i$ and $\mu_i$ denotes the disease-induced death rate in patch $i$. The infection rate $\sigma_i$

in patch $i$ have the form below as:

$$\sigma_i = \sum_{j=1}^{n} \beta_j W_{ij} \frac{\sum_{k=1}^{n} W_{kj} I_k}{\sum_{k=1}^{n} W_{kj} N_k}$$

with $W_{ij}$ denotes the proportion of individuals from patch $i$ who are currently in patch $j$ , $\beta_j$ is the risk of infection in patch $j$ , and the last fraction represents the proportion of infected in patch $j$.

According to the above system of differential equations, it is first necessary to determine the parameters $\alpha_i, \mu_i$ and $\beta_i$ for each province $i$.

| | Duration | No. of Cases | No. of Deaths | Case* Fatality Rate |
|---|---|---|---|---|
| 1st wave | 27.01.2020-03.10.2020 | 3,396 | 13 | 0.38 |
| 2nd wave | 04.10.2020-14.04.2021 | 92,341 | 591 | 0.64 |
| 3rd wave | 15.04.2021-31.12.2022 | 576,434 | 16,238 | 2.81 |

Figure 4.1: Disease-induced death rate (fatality rate) of COVID-19 for different durations.

According to the Figure 4.1 the mean fatality rate is $\frac{0.38+0.64+2.81}{3} = 0.012766666$. This parameter is assumed to be primarily biological and, therefore, fixed over time and the same in all countries and regions [28]. It allows to take the disease-induced death rate for all provinces in Sri Lanka is considered as a fixed parameter, i.e., $\mu_i = 0.012766666$ for each province $i$.

Moreover, Sri Lanka is a small island with a small crowd of population compared to some other big countries like India, the USA, Russia, etc. Therefore, the recovery rates $\alpha_i$ of the humans in province $i$ for all nine provinces are assumed to be the same, i.e., $\alpha_i^{-1} = 10.25$ days for each province $i$ [44; 45]. Furthermore, the risk of infection in province $j$ i.e., $\beta_j$ found in [44] for each province $j$ below as:

| Symbol | Province | Value |
|---|---|---|
| $\beta_1$ | Central | 0.11607572 |
| $\beta_2$ | Eastern | 0.00972736 |
| $\beta_3$ | North central | 0.02554977 |
| $\beta_4$ | North western | 0.13890953 |
| $\beta_5$ | Northern | 0.07344980 |
| $\beta_6$ | Sabaragamuwa | 0.00473791 |
| $\beta_7$ | Southern | 0.11356019 |
| $\beta_8$ | Uva | 0.00020758 |
| $\beta_9$ | Western | 0.12895880 |

Table 4.1: This table shows the risk of infection in each province in Sri Lanka for COVID-19.

| Index | Province | $S_i(0)$ (in thousands) | $I_i(0)$ | $R_i(0)$ | $D_i(0)$ |
|---|---|---|---|---|---|
| 1 | Central | 2781 | 0 | 0 | 0 |
| 2 | Eastern | 1746 | 1 | 0 | 0 |
| 3 | North central | 1386 | 0 | 0 | 0 |
| 4 | North western | 2563 | 16 | 0 | 0 |
| 5 | Northern | 1152 | 0 | 0 | 0 |
| 6 | Sabaragamuwa | 2070 | 4 | 0 | 0 |
| 7 | Southern | 2669 | 2 | 0 | 0 |
| 8 | Uva | 1387 | 1 | 0 | 0 |
| 9 | Western | 6165 | 39 | 0 | 0 |

Table 4.2: The initial distribution of Susceptible, Infected, Recovered and Dead for each province.

The Table 4.2 shows the initial distribution of $(S_i(t), I_i(t), R_i(t), D_i(t))$ for

each province $i$, assuming the spread of COVID-19 starts in 2020-03-20 ($t = 0$) in Sri Lanka and initially there are no recovered and disease-induced death individuals, according to the limitations of data.

Moreover, the proportion of individuals from patch $i$ who are currently in patch $j$, i.e., $W_{ij}$ values are shown in the Tables A.19-A.27 for each pair of provinces.

## 4.3 Results of Multi-Patch SIRD Model

According to the above data, solve the multi-patch SIRD model and the distributions of $I_i(t)$ starting from 2020-03-20 are shown in the below figures for each province $i$.

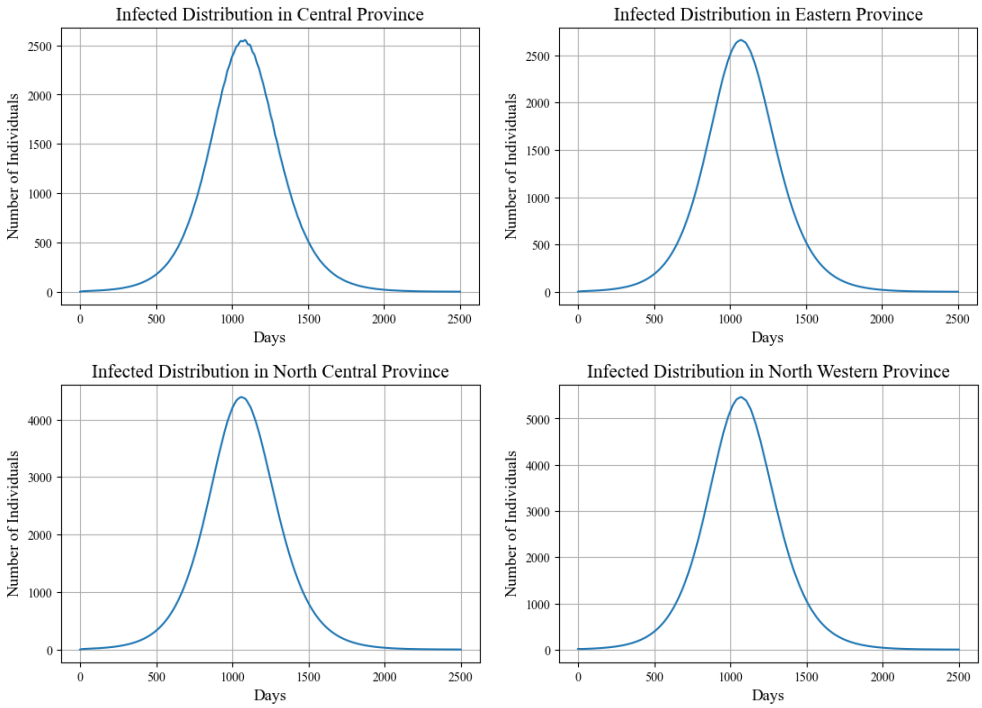


Figure 4.2: Infected distribution of Central, Eastern, North central and North western provinces starting from 2020-03-20

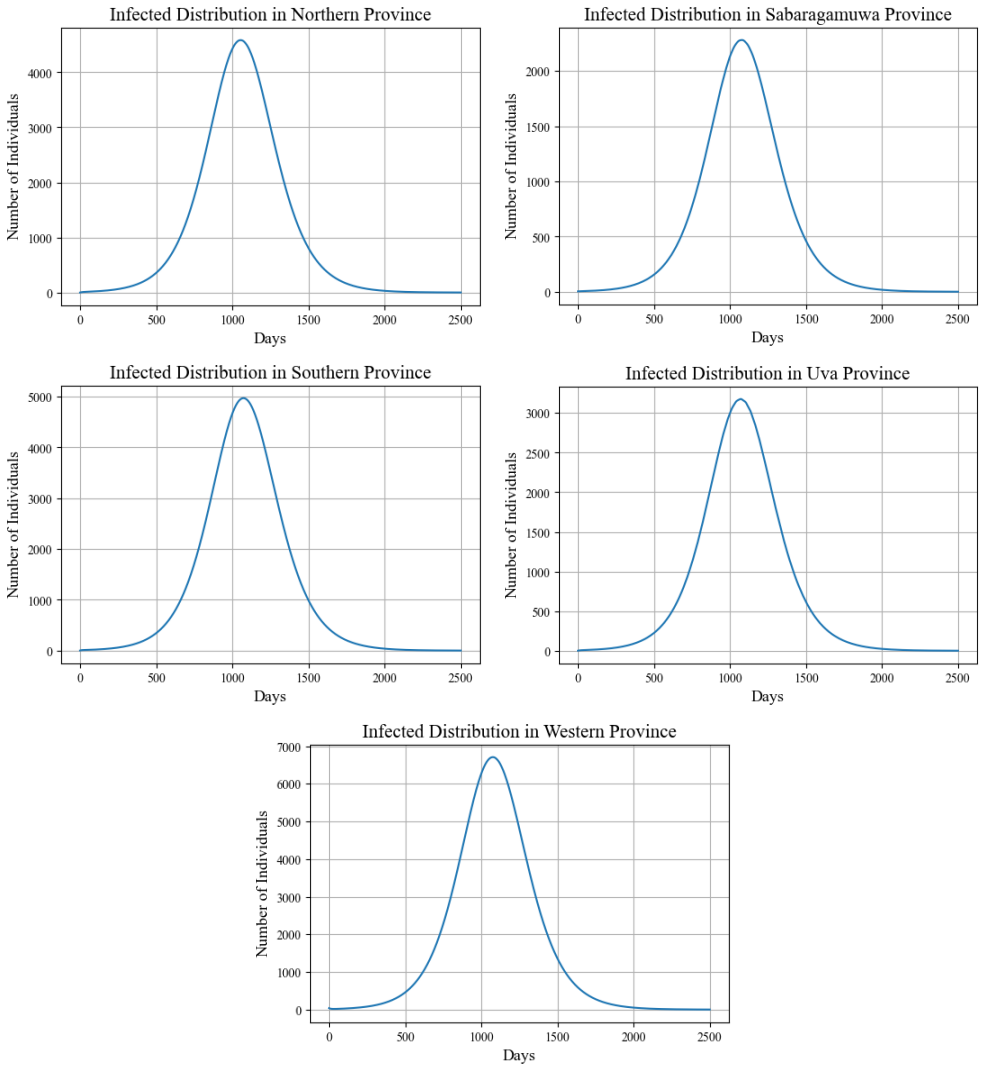


Figure 4.3: Infected distribution of Northern, Sabaragamuwa, Southern, Uva, Western provinces starting from 2020-03-20

# Chapter 5

# Conclusions

An important limitation of the radiation model is that it cannot capture human mobility restrictions, such as lockdowns or quarantines, when used to predict human mobility between patches. Therefore, the above infected distributions in Figures 4.2,4.3 show how human mobility impacts the spread of COVID-19 between provinces without considering human mobility restrictions. Moreover, Figures 4.2,4.3 illustrates how COVID-19 could spread in the absence of mobility restrictions such as lockdowns. Therefore, the integration of these mathematical models with epidemiology not only helps to understand the spread of infectious diseases, but it also helps in current and future decision-making in public health. Moreover, this method can be used to study how human mobility impacts the spread of any human-to-human infectious disease without considering human mobility restrictions when there is a lack of systematic mobility data.

The analysis in Section 3.1 shows, the distance exponent $\gamma$ in modified gravity model as a function of the fractal dimension $d_f$ and the power-law exponent $\beta$ of the population distribution, the potential to attract movement $\omega$ of the modified gravity model and the distance $r_{ij}$ between origin $i$ and destination $j$ patches. Moreover, it shows this distance exponent function can vary according

to the population of origin $m_i$ and destination $m_j$ patches such as Equations 3.14,3.18,3.21. This strongly implies that a given data set does not necessarily have to be characterized by the single value of the distance exponent, and it depends on the properties of the population landscape. Moreover, these results can be used to study human mobility when there is a lack of systematic mobility data.

This paper [44] provides the study of formulating a multi-patch epidemic model via a gravity model approach by identifying a way to model human dispersal behaviors within a patch using the gravity model. Moreover, the above study goes through the spread of COVID-19 between provinces in Sri Lanka. Combining both of these studies ([44] and "Gravity Model Explained by the Radiation Model in Modeling Epidemics") provides the opportunity to compare the effectiveness of the gravity model with the radiation model in modeling the spread of infectious diseases as future work.

# Appendix A

# Tables

## A.1 Estimated Values in Section 3.2.2

| Origin | Destination | Distance (m) | Surrounding population |
|---|---|---|---|
| Central | Central | 0 | 0 |
| Central | Eastern | 111889.883 | 13571 |
| Central | North central | 102870.023 | 12185 |
| Central | North western | 71029.657 | 3457 |
| Central | Northern | 246331.336 | 17986 |
| Central | Sabaragamuwa | 50874.174 | 0 |
| Central | Southern | 124345.218 | 15317 |
| Central | Uva | 61511.067 | 2070 |
| Central | Western | 84734.014 | 6020 |

Table A.1: Distance from Central province (index:1) to each province and the surrounding population (in thousands) of Central province for each destination.

.

| Origin | Destination | Distance (m) | Surrounding population |
|---|---|---|---|
| Eastern | Central | 111889.883 | 2773 |
| Eastern | Eastern | 0 | 0 |
| Eastern | North central | 107456.990 | 1387 |
| Eastern | North western | 156341.849 | 5554 |
| Eastern | Northern | 238025.296 | 19021 |
| Eastern | Sabaragamuwa | 156741.364 | 8117 |
| Eastern | Southern | 212352.846 | 16352 |
| Eastern | Uva | 104858.660 | 0 |
| Eastern | Western | 196574.756 | 10187 |

Table A.2: Distance from Eastern province (index:2) to each province and the surrounding population (in thousands) of Eastern province for each destination.

| Origin | Destination | Distance (m) | Surrounding population |
|---|---|---|---|
| North central | Central | 102870.023 | 2563 |
| North central | Eastern | 107456.990 | 5344 |
| North central | North central | 0 | 0 |
| North central | North western | 86060.023 | 0 |
| North central | Northern | 147697.922 | 7090 |
| North central | Sabaragamuwa | 150239.717 | 9629 |
| North central | Southern | 226689.950 | 17864 |
| North central | Uva | 148378.729 | 8242 |
| North central | Western | 160691.718 | 11699 |

Table A.3: Distance from North central province (index:3) to each province and the surrounding population (in thousands) of North central province for each destination.

| Origin | Destination | Distance (m) | Surrounding population |
|---|---|---|---|
| North western | Central | 71029.657 | 0 |
| North western | Eastern | 156341.849 | 13789 |
| North western | North central | 86060.023 | 8946 |
| North western | North western | 0 | 0 |
| North western | Northern | 200429.418 | 18204 |
| North western | Sabaragamuwa | 93052.714 | 10332 |
| North western | Southern | 168409.261 | 15535 |
| North western | Uva | 132496.626 | 12402 |
| North western | Western | 80815.904 | 2781 |

Table A.4: Distance from North western province (index:4) to each province and the surrounding population (in thousands) of North western province for each destination.

| Origin | Destination | Distance (m) | Surrounding population |
|---|---|---|---|
| Northern | Central | 246331.336 | 5695 |
| Northern | Eastern | 238025.296 | 3949 |
| Northern | North central | 147697.922 | 0 |
| Northern | North western | 200429.418 | 1386 |
| Northern | Northern | 0 | 0 |
| Northern | Sabaragamuwa | 287777.135 | 14641 |
| Northern | Southern | 365406.551 | 18098 |
| Northern | Uva | 296023.699 | 16711 |
| Northern | Western | 280301.386 | 8476 |

Table A.5: Distance from Northern province (index:5) to each province and the surrounding population (in thousands) of Northern province for each destination.

| Origin | Destination | Distance (m) | Surrounding population |
|---|---|---|---|
| Sabaragamuwa | Central | 50874.174 | 0 |
| Sabaragamuwa | Eastern | 156741.364 | 16951 |
| Sabaragamuwa | North central | 150239.717 | 15565 |
| Sabaragamuwa | North western | 93052.714 | 13002 |
| Sabaragamuwa | Northern | 287777.135 | 18697 |
| Sabaragamuwa | Sabaragamuwa | 0 | 0 |
| Sabaragamuwa | Southern | 77679.418 | 10333 |
| Sabaragamuwa | Uva | 71864.447 | 8946 |
| Sabaragamuwa | Western | 53173.148 | 2781 |

Table A.6: Distance from Sabaragamuwa province (index:6) to each province and the surrounding population (in thousands) of Sabaragamuwa province for each destination.

| Origin | Destination | Distance (m) | Surrounding population |
|---|---|---|---|
| Southern | Central | 124345.218 | 9622 |
| Southern | Eastern | 212352.846 | 14966 |
| Southern | North central | 226689.950 | 16712 |
| Southern | North western | 168409.2614 | 12403 |
| Southern | Northern | 365406.551 | 18098 |
| Southern | Sabaragamuwa | 77679.418 | 0 |
| Southern | Southern | 0 | 0 |
| Southern | Uva | 108365.580 | 8235 |
| Southern | Western | 102195.596 | 2070 |

Table A.7: Distance from Southern province (index:7) to each province and the surrounding population (in thousands) of Southern province for each destination.

| Origin | Destination | Distance (m) | Surrounding population |
|---|---|---|---|
| Uva | Central | 61511.067 | 0 |
| Uva | Eastern | 104858.660 | 4851 |
| Uva | North central | 148378.729 | 17994 |
| Uva | North western | 132496.626 | 15431 |
| Uva | Northern | 296023.699 | 19380 |
| Uva | Sabaragamuwa | 71864.447 | 2781 |
| Uva | Southern | 108365.580 | 6597 |
| Uva | Uva | 0 | 0 |
| Uva | Western | 124146.937 | 9266 |

Table A.8: Distance from Uva province (index:8) to each province and the surrounding population (in thousands) of Uva province for each destination.

| Origin | Destination | Distance (m) | Surrounding population |
|---|---|---|---|
| Western | Central | 84734.014 | 4633 |
| Western | Eastern | 196574.756 | 12856 |
| Western | North central | 160691.718 | 11470 |
| Western | North western | 80815.904 | 2070 |
| Western | Northern | 280301.386 | 14602 |
| Western | Sabaragamuwa | 53173.148 | 0 |
| Western | Southern | 102195.596 | 7414 |
| Western | Uva | 124146.937 | 10083 |
| Western | Western | 0 | 0 |

Table A.9: Distance from Western province (index:9) to each province and the surrounding population (in thousands) of Western province for each destination.

## A.2 Estimated Values in Section 3.2.3

| Origin | Destination | Travel probability $P^*_{ij}$ | Normalized travel probability |
|---|---|---|---|
| Central | Central | 0.57265649 | 0.36413323 |
| Central | Eastern | 0.01879178 | 0.01194907 |
| Central | North central | 0.01803897 | 0.01147038 |
| Central | North western | 0.14869501 | 0.09455021 |
| Central | Northern | 0.00806089 | 0.00512565 |
| Central | Sabaragamuwa | 0.48872354 | 0.31076306 |
| Central | Southern | 0.02261879 | 0.01438254 |
| Central | Uva | 0.14599063 | 0.09283059 |
| Central | Western | 0.14908038 | 0.09479526 |

Table A.10: The travel probability from Central province (index:1) to each destination.

| Origin | Destination | Travel probability $P^*_{ij}$ | Normalized travel probability |
|---|---|---|---|
| Eastern | Central | 0.16167745 | 0.10511443 |
| Eastern | Eastern | 0.53793906 | 0.34974055 |
| Eastern | North central | 0.18632981 | 0.12114214 |
| Eastern | North western | 0.06861241 | 0.04460829 |
| Eastern | Northern | 0.00490763 | 0.00319069 |
| Eastern | Sabaragamuwa | 0.0339753 | 0.022089 |
| Eastern | Southern | 0.01376521 | 0.00894944 |
| Eastern | Uva | 0.47565068 | 0.30924382 |
| Eastern | Western | 0.05525139 | 0.03592163 |

Table A.11: The travel probability from Eastern province (index:2) to each destination.

| Origin | Destination | Travel probability $P_{ij}^*$ | Normalized travel probability |
|---|---|---|---|
| North central | Central | 0.15595273 | 0.10189617 |
| North central | Eastern | 0.0457407 | 0.029886 |
| North central | North central | 0.53044379 | 0.34658061 |
| North central | North western | 0.69001585 | 0.45084156 |
| North central | Northern | 0.02111434 | 0.01379566 |
| North central | Sabaragamuwa | 0.02150492 | 0.01405085 |
| North central | Southern | 0.00948477 | 0.00619715 |
| North central | Uva | 0.01957238 | 0.01278818 |
| North central | Western | 0.03667678 | 0.02396382 |

Table A.12: The travel probability from North central province (index:3) to each destination.

| Origin | Destination | Travel probability $P_{ij}^*$ | Normalized travel probability |
|---|---|---|---|
| North western | Central | 0.58700316 | 0.37531125 |
| North western | Eastern | 0.01728499 | 0.01105148 |
| North western | North central | 0.02732292 | 0.01746941 |
| North western | North western | 0.56386641 | 0.36051834 |
| North western | Northern | 0.0074194 | 0.00474373 |
| North western | Sabaragamuwa | 0.03140127 | 0.02007698 |
| North western | Southern | 0.02081297 | 0.01330716 |
| North western | Uva | 0.01660007 | 0.01061356 |
| North western | Western | 0.29233243 | 0.1869081 |

Table A.13: The travel probability from North western province (index:4) to each destination.

| Origin | Destination | Travel probability $P_{ij}^*$ | Normalized travel probability |
|---|---|---|---|
| Northern | Central | 0.05200831 | 0.0341362 |
| Northern | Eastern | 0.06151185 | 0.04037394 |
| Northern | North central | 0.57224144 | 0.37559664 |
| Northern | North western | 0.24233889 | 0.15906166 |
| Northern | Northern | 0.52349903 | 0.34360405 |
| Northern | Sabaragamuwa | 0.00907086 | 0.00595375 |
| Northern | Southern | 0.00782334 | 0.00513493 |
| Northern | Uva | 0.0049876 | 0.00327367 |
| Northern | Western | 0.05007182 | 0.03286516 |

Table A.14: The travel probability from Northern province (index:5) to each destination.

| Origin | Destination | Travel probability $P^*_{ij}$ | Normalized travel probability |
|---|---|---|---|
| Sabaragamuwa | Central | 0.63100897 | 0.4070921 |
| Sabaragamuwa | Eastern | 0.01019565 | 0.00657767 |
| Sabaragamuwa | North central | 0.00952915 | 0.00614768 |
| Sabaragamuwa | North western | 0.0222319 | 0.01434279 |
| Sabaragamuwa | Northern | 0.00583847 | 0.00376666 |
| Sabaragamuwa | Sabaragamuwa | 0.54993892 | 0.35479018 |
| Sabaragamuwa | Southern | 0.03290087 | 0.02122582 |
| Sabaragamuwa | Uva | 0.02338083 | 0.01508402 |
| Sabaragamuwa | Western | 0.2650151 | 0.17097309 |

Table A.15: The travel probability from Sabaragamuwa province (index:6) to each destination.

| Origin | Destination | Travel probability $P^*_{ij}$ | Normalized travel probability |
|---|---|---|---|
| Southern | Central | 0.04604146 | 0.02938173 |
| Southern | Eastern | 0.01568781 | 0.0100113 |
| Southern | North central | 0.01057804 | 0.00675046 |
| Southern | North western | 0.02959791 | 0.01888814 |
| Southern | Northern | 0.00777563 | 0.00496208 |
| Southern | Sabaragamuwa | 0.49477193 | 0.31574274 |
| Southern | Southern | 0.56679834 | 0.36170697 |
| Southern | Uva | 0.03171371 | 0.02023836 |
| Southern | Western | 0.36404488 | 0.2323182 |

Table A.16: The travel probability from Southern province (index:7) to each destination.

| Origin | Destination | Travel probability $P^*_{ij}$ | Normalized travel probability |
|---|---|---|---|
| Uva | Central | 0.70945447 | 0.46358236 |
| Uva | Eastern | 0.05243418 | 0.03426233 |
| Uva | North central | 0.0051706 | 0.00337865 |
| Uva | North western | 0.01180381 | 0.00771303 |
| Uva | Northern | 0.00380049 | 0.00248337 |
| Uva | Sabaragamuwa | 0.1187932 | 0.07762363 |
| Uva | Southern | 0.04699986 | 0.03071135 |
| Uva | Uva | 0.53030845 | 0.34652209 |
| Uva | Western | 0.05160908 | 0.03372318 |

Table A.17: The travel probability from Uva province (index:8) to each destination.

| Origin | Destination | Travel probability $P_{ij}^{*}$ | Normalized travel probability |
|---|---|---|---|
| Western | Central | 0.16311167 | 0.09617864 |
| Western | Eastern | 0.03812244 | 0.02247886 |
| Western | North central | 0.03562336 | 0.02100528 |
| Western | North western | 0.24735889 | 0.14585493 |
| Western | Northern | 0.02183404 | 0.01287442 |
| Western | Sabaragamuwa | 0.34884862 | 0.20569824 |
| Western | Southern | 0.10417599 | 0.06142727 |
| Western | Uva | 0.04171676 | 0.02459825 |
| Western | Western | 0.69513238 | 0.40988412 |

Table A.18: The travel probability from Western province (index:9) to each destination.

## A.3 Estimated Values in Section 3.3

| Origin | Destination | $W_{ij}$ | Normalized value |
|---|---|---|---|
| Central | Central | 0.30161059 | 0.36413323 |
| Central | Eastern | 0.00989738 | 0.01194907 |
| Central | North central | 0.00950089 | 0.01147038 |
| Central | North western | 0.07831569 | 0.09455021 |
| Central | Northern | 0.00424557 | 0.00512565 |
| Central | Sabaragamuwa | 0.25740422 | 0.31076306 |
| Central | Southern | 0.01191302 | 0.01438254 |
| Central | Uva | 0.07689133 | 0.09283059 |
| Central | Western | 0.07851866 | 0.09479526 |

Table A.19: The proportion of individuals from the Central province (index:1) who are currently in each province.

| Origin | Destination | $W_{ij}$ | Normalized value |
|---|---|---|---|
| Eastern | Central | 0.08515337 | 0.10511443 |
| Eastern | Eastern | 0.28332538 | 0.34974055 |
| Eastern | North central | 0.09813744 | 0.12114214 |
| Eastern | North western | 0.03613725 | 0.04460829 |
| Eastern | Northern | 0.00258479 | 0.00319069 |
| Eastern | Sabaragamuwa | 0.01789434 | 0.022089 |
| Eastern | Southern | 0.00724996 | 0.00894944 |
| Eastern | Uva | 0.25051891 | 0.30924382 |
| Eastern | Western | 0.02910017 | 0.03592163 |

Table A.20: The proportion of individuals from the Eastern province (index:2) who are currently in each province.

| Origin | Destination | $W_{ij}$ | Normalized value |
|---|---|---|---|
| North central | Central | 0.08213824 | 0.10189617 |
| North central | Eastern | 0.02409102 | 0.029886 |
| North central | North central | 0.27937772 | 0.34658061 |
| North central | North western | 0.36342221 | 0.45084156 |
| North central | Northern | 0.01112064 | 0.01379566 |
| North central | Sabaragamuwa | 0.01132636 | 0.01405085 |
| North central | Southern | 0.0049955 | 0.00619715 |
| North central | Uva | 0.01030851 | 0.01278818 |
| North central | Western | 0.01931718 | 0.02396382 |

Table A.21: The proportion of individuals from the North central province (index:3) who are currently in each province.

| Origin | Destination | $W_{ij}$ | Normalized value |
|---|---|---|---|
| North western | Central | 0.30916679 | 0.37531125 |
| North western | Eastern | 0.00910378 | 0.01105148 |
| North western | North central | 0.01439062 | 0.01746941 |
| North western | North western | 0.29698097 | 0.36051834 |
| North western | Northern | 0.0039077 | 0.00474373 |
| North western | Sabaragamuwa | 0.01653863 | 0.02007698 |
| North western | Southern | 0.01096192 | 0.01330716 |
| North western | Uva | 0.00874304 | 0.01061356 |
| North western | Western | 0.15396762 | 0.1869081 |

Table A.22: The proportion of individuals from the North western province (index:4) who are currently in each province.

| Origin | Destination | $W_{ij}$ | Normalized value |
|---|---|---|---|
| Northern | Central | 0.02739209 | 0.0341362 |
| Northern | Eastern | 0.03239747 | 0.04037394 |
| Northern | North central | 0.30139199 | 0.37559664 |
| Northern | North western | 0.12763669 | 0.15906166 |
| Northern | Northern | 0.27572001 | 0.34360405 |
| Northern | Sabaragamuwa | 0.0047775 | 0.00595375 |
| Northern | Southern | 0.00412045 | 0.00513493 |
| Northern | Uva | 0.0026269 | 0.00327367 |
| Northern | Western | 0.02637217 | 0.03286516 |

Table A.23: The proportion of individuals from the Northern province (index:5) who are currently in each province.

| Origin | Destination | $W_{ij}$ | Normalized value |
|---|---|---|---|
| Sabaragamuwa | Central | 0.33234407 | 0.4070921 |
| Sabaragamuwa | Eastern | 0.00536991 | 0.00657767 |
| Sabaragamuwa | North central | 0.00501888 | 0.00614768 |
| Sabaragamuwa | North western | 0.01170925 | 0.01434279 |
| Sabaragamuwa | Northern | 0.00307504 | 0.00376666 |
| Sabaragamuwa | Sabaragamuwa | 0.28964555 | 0.35479018 |
| Sabaragamuwa | Southern | 0.01732845 | 0.02122582 |
| Sabaragamuwa | Uva | 0.01231437 | 0.01508402 |
| Sabaragamuwa | Western | 0.13957994 | 0.17097309 |

Table A.24: The proportion of individuals from the Sabaragamuwa province (index:6) who are currently in each province.

| Origin | Destination | $W_{ij}$ | Normalized value |
|---|---|---|---|
| Southern | Central | 0.02424943 | 0.02938173 |
| Southern | Eastern | 0.00826256 | 0.0100113 |
| Southern | North central | 0.00557132 | 0.00675046 |
| Southern | North western | 0.01558882 | 0.01888814 |
| Southern | Northern | 0.00409532 | 0.00496208 |
| Southern | Sabaragamuwa | 0.26058983 | 0.31574274 |
| Southern | Southern | 0.29852518 | 0.36170697 |
| Southern | Uva | 0.01670319 | 0.02023836 |
| Southern | Western | 0.19173762 | 0.2323182 |

Table A.25: The proportion of individuals from the Southern province (index:7) who are currently in each province.

| Origin | Destination | $W_{ij}$ | Normalized value |
|---|---|---|---|
| Uva | Central | 0.37366027 | 0.46358236 |
| Uva | Eastern | 0.02761639 | 0.03426233 |
| Uva | North central | 0.00272328 | 0.00337865 |
| Uva | North western | 0.00621691 | 0.00771303 |
| Uva | Northern | 0.00200167 | 0.00248337 |
| Uva | Sabaragamuwa | 0.06256681 | 0.07762363 |
| Uva | Southern | 0.02475421 | 0.03071135 |
| Uva | Uva | 0.27930644 | 0.34652209 |
| Uva | Western | 0.02718182 | 0.03372318 |

Table A.26: The proportion of individuals from the Uva province (index:8) who are currently in each province.

| Origin | Destination | $W_{ij}$ | Normalized value |
|---|---|---|---|
| Western | Central | 0.08590876 | 0.09617864 |
| Western | Eastern | 0.02007858 | 0.02247886 |
| Western | North central | 0.01876235 | 0.02100528 |
| Western | North western | 0.13028065 | 0.14585493 |
| Western | Northern | 0.0114997 | 0.01287442 |
| Western | Sabaragamuwa | 0.18373395 | 0.20569824 |
| Western | Southern | 0.05486811 | 0.06142727 |
| Western | Uva | 0.02197167 | 0.02459825 |
| Western | Western | 0.36611702 | 0.40988412 |

Table A.27: The proportion of individuals from the Western province (index:9) who are currently in each province.

# Appendix B

# Programming Codes and Data Sources

- The population density in 2020 in Sri Lanka, which was generated by the raster data format
  - `https://www.worldpop.org`
- Shapefile of Sri Lanka with districts
  - `https://diva-gis.org/data.html`
- Population of each province in 2020
  - visit data set
- Number of commuters in Sri Lanka
  - visit data set
- Infected individuals in each province on 2020-03-20 and Figure 4.1
  - visit data set
- Programming codes of section 2.1.4, 2.1.6, 3.2.1, 3.2.2, 3.2.3, 3.3 and 4.3
  - GitHub

# References


[1] T. L. Hale and G. T. Keusch, "Shigella," *Medical Microbiology. 4th edition*, 1996. 1

[2] J. Zhang, B. Feng, Y. Wu, P. Xu, R. Ke, and N. Dong, "The effect of human mobility and control measures on traffic safety during covid-19 pandemic," *PLoS one*, vol. 16, no. 3, p. e0243263, 2021. 1

[3] Y. Bali, V. P. Bajiya, J. P. Tripathi, and A. Mubayi, "Exploring data sources and mathematical approaches for estimating human mobility rates and implications for understanding covid-19 dynamics: a systematic literature review," *Journal of Mathematical Biology*, vol. 88, no. 6, p. 67, 2024. 2

[4] K. Sallah, R. Giorgi, L. Bengtsson, X. Lu, E. Wetter, P. Adrien, S. Rebaudet, R. Piarroux, and J. Gaudart, "Mathematical models for predicting human mobility in the context of infectious disease spread: introducing the impedance model," *International journal of health geographics*, vol. 16, pp. 1–11, 2017. 2

[5] H. Barbosa, M. Barthelemy, G. Ghoshal, C. R. James, M. Lenormand, T. Louail, R. Menezes, J. J. Ramasco, F. Simini, and M. Tomasini, "Human mobility: Models and applications," *Physics Reports*, vol. 734, pp. 1–74, 2018. 2

[6] D. Bichara and A. Iggidr, "Multi-patch and multi-group epidemic models: a

new framework," *Journal of mathematical biology*, vol. 77, no. 1, pp. 107–134, 2018. 2, 27

[7] F. Brauer, C. Castillo-Chavez, Z. Feng, F. Brauer, C. Castillo-Chavez, and Z. Feng, "Epidemiological models incorporating mobility, behavior, and time scales," *Mathematical Models in Epidemiology*, pp. 477–504, 2019. 2, 26, 27

[8] M. De Rooij, "The analysis of change, newton's law of gravity and association models," *Journal of the Royal Statistical Society Series A: Statistics in Society*, vol. 171, no. 1, pp. 137–157, 2008. 6

[9] K. E. Haynes and A. S. Fotheringham, "Gravity and spatial interaction models," 2020. 8, 9

[10] F. Simini, M. C. González, A. Maritan, and A.-L. Barabási, "A universal model for mobility and migration patterns," *Nature*, vol. 484, no. 7392, pp. 96–100, 2012. 8, 9, 10, 11, 12, 30

[11] I. Hong, W.-S. Jung, and H.-H. Jo, "Gravity model explained by the radiation model on a population landscape," *PloS one*, vol. 14, no. 6, p. e0218028, 2019. 11, 12, 22, 28, 31

[12] M. Stefanouli and S. Polyzos, "Gravity vs radiation model: two approaches on commuting in greece," *Transportation research procedia*, vol. 24, pp. 65–72, 2017. 11

[13] A. Clauset, C. R. Shalizi, and M. E. Newman, "Power-law distributions in empirical data," *SIAM review*, vol. 51, no. 4, pp. 661–703, 2009. 15

[14] K. T. Soo, "Zipf's law for cities: a cross-country investigation," *Regional science and urban Economics*, vol. 35, no. 3, pp. 239–263, 2005. 15

[15] D.-S. Lee, K.-I. Goh, B. Kahng, and D. Kim, "Sandpile avalanche dynamics on scale-free networks," *Physica A: Statistical Mechanics and its Applications*, vol. 338, no. 1-2, pp. 84–91, 2004. 15

[16] M. E. Newman, "A model of mass extinction," *Journal of theoretical Biology*, vol. 189, no. 3, pp. 235–252, 1997. 15

[17] X. Gabaix and Y. M. Ioannides, "The evolution of city size distributions," in *Handbook of regional and urban economics*, vol. 4, pp. 2341–2378, Elsevier, 2004. 15

[18] N. Masseran, L. H. Yee, M. A. M. Safari, and K. Ibrahim, "Power law behavior and tail modeling on low income distribution," *Mathematics and Statistics*, vol. 7, no. 3, pp. 70–77, 2019. 15

[19] M. Sajid, A. Husain, J. Reddy, M. T. Alresheedi, S. A. Al Yahya, and A. Al-Rajy, "Box dimension of the border of kingdom of saudi arabia," *Heliyon*, vol. 9, no. 4, 2023. 15

[20] B. MELLOR, "Fractals: Self-similarity and fractal dimension math 198, spring 2013." 15, 16, 17, 18

[21] K. E. Chlouverakis and J. Sprott, "A comparison of correlation and lyapunov dimensions," *Physica D: Nonlinear Phenomena*, vol. 200, no. 1-2, pp. 156–164, 2005. 15

[22] D. Schleicher, "Hausdorff dimension, its properties, and its surprises," *The American Mathematical Monthly*, vol. 114, no. 6, pp. 509–528, 2007. 15

[23] Q. Kuang, "Fractal dimension: introduction, example, and application," 2024. 19

[24] R. Soneira and P. Peebles, "A computer model universe-simulation of the nature of the galaxy distribution in the lick catalog," *Astronomical Journal, vol. 83, July 1978, p. 845-860. NSF-supported research.*, vol. 83, pp. 845–860, 1978. 19

[25] D. Gospodinov, A. Marinov, and E. Marekova, "Testing fractal coefficients sensitivity on real and simulated earthquake data," *Acta Geophysica*, vol. 60, pp. 794–808, 2012. 19, 20

[26] W. O. Kermack and A. G. McKendrick, "A contribution to the mathematical theory of epidemics," *Proceedings of the royal society of london. Series A, Containing papers of a mathematical and physical character*, vol. 115, no. 772, pp. 700–721, 1927. 23

[27] W. O. Kermack and A. G. McKendrick, "Contributions to the mathematical theory of epidemics. ii.—the problem of endemicity," *Proceedings of the Royal Society of London. Series A, containing papers of a mathematical and physical character*, vol. 138, no. 834, pp. 55–83, 1932. 23

[28] J. Fernández-Villaverde and C. I. Jones, "Estimating and simulating a sird model of covid-19 for many countries, states, and cities," *Journal of Economic Dynamics and Control*, vol. 140, p. 104318, 2022. 23, 26, 66

[29] H. W. Hethcote, "The mathematics of infectious diseases," *SIAM review*, vol. 42, no. 4, pp. 599–653, 2000. 23

[30] R. Morton and K. H. Wickwire, "On the optimal control of a deterministic epidemic," *Advances in Applied Probability*, vol. 6, no. 4, pp. 622–635, 1974. 23

[31] F. Brauer, C. Castillo-Chavez, Z. Feng, *et al.*, *Mathematical models in epidemiology*, vol. 32. Springer, 2019. 23

[32] N. M. Ferguson, D. Laydon, G. Nedjati-Gilani, N. Imai, K. Ainslie, M. Baguelin, S. Bhatia, A. Boonyasiri, Z. Cucunubá, G. Cuomo-Dannenburg, *et al.*, *Report 9: Impact of non-pharmaceutical interventions (NPIs) to reduce COVID19 mortality and healthcare demand*, vol. 16. Imperial College London London, 2020. 23

[33] C. Cakmaklı and Y. Şimşek, "Bridging the covid-19 data and the epidemiological model using the time-varying parameter sird model," *Journal of Econometrics*, vol. 242, no. 1, p. 105787, 2024. 24, 26

[34] N. S. Rustum and S. A. S. Al-Temimi, "Estimation of the epidemiological model with a system of differential equations (sird) using the runge-kutta method in iraq," *International Journal of Nonlinear Analysis and Applications*, vol. 13, no. 2, pp. 2807–2814, 2022. 24, 25, 26

[35] C. Pacheco and C. de Lacerda, "Function estimation and regularization in the sird model applied to the covid-19 pandemics," *Inverse Problems in Science and Engineering*, vol. 29, no. 11, pp. 1613–1628, 2021. 26

[36] D. Caccavo, "Chinese and italian covid-19 outbreaks can be correctly described by a modified sird model," *MedRxiv*, pp. 2020–03, 2020. 26

[37] D. Bichara and C. Castillo-Chavez, "Vector-borne diseases models with residence times–a lagrangian perspective," *Mathematical biosciences*, vol. 281, pp. 128–138, 2016. 27

[38] C. Castillo-Chavez, D. Bichara, and B. R. Morin, "Perspectives on the role of mobility, behavior, and time scales in the spread of diseases," *Proceedings of the National Academy of Sciences*, vol. 113, no. 51, pp. 14582–14588, 2016. 27

[39] D. Bichara, Y. Kang, C. Castillo-Chavez, R. Horan, and C. Perrings, "Sis and sir epidemic models under virtual dispersal," *Bulletin of mathematical biology*, vol. 77, pp. 2004–2034, 2015. 27

[40] R. C. Corgel, *Characterizing the Impact of Integrating Spatially Aggregated Human Mobility Data into Infectious Disease Models.* PhD thesis, Johns Hopkins University, 2023. 28

[41] A. P. Masucci, J. Serras, A. Johansson, and M. Batty, "Gravity versus radiation models: On the importance of scale and heterogeneity in commuting flows," *Physical Review E—Statistical, Nonlinear, and Soft Matter Physics*, vol. 88, no. 2, p. 022812, 2013. 43

[42] D. S. Ediriweera, N. R. De Silva, G. N. Malavige, and H. J. De Silva, "An epidemiological model to aid decision-making for covid-19 control in sri lanka," *PLoS One*, vol. 15, no. 8, p. e0238340, 2020. 63, 64, 65

[43] J. M. Heffernan, R. J. Smith, and L. M. Wahl, "Perspectives on the basic reproductive ratio," *Journal of the Royal Society Interface*, vol. 2, no. 4, pp. 281–293, 2005. 64

[44] A. Dinasiri and Y. . Jayathunga, "Gravity model approach to model epidemic with human dispersal behaviors," *Communication in Biomathematical Sciences, 7(2), pp. 232-248. doi: 10.5614/cbms.2024.7.2.5.*, 2024.12.31. 67, 71

[45] K. Erandi, A. C. Mahasinghe, S. Perera, and S. Jayasinghe, "Effectiveness of the strategies implemented in sri lanka for controlling the covid-19 outbreak," *Journal of Applied Mathematics*, vol. 2020, no. 1, p. 2954519, 2020. 67

[46] G. Dmap, I. A. Abeyagunwardena, S. S. Manathunga, M. Galhena, S. Ginige,

and S. Dharmaratne, "Covid-19 deaths in sri lanka-implications for global health," *Available at SSRN 4597984*, 2023.